HOKKAIDO UNIVERSITY

Title	Microscopic formulation of the interacting boson-fermion model using the nuclear energy density functional
Author(s)	Homma, M.; Nomura, K.
Citation	Physical Review C, 113(6) https://doi.org/10.1103/2km2-s25q
Issue Date	2026-06-01
Doc URL	https://hdl.handle.net/2115/100018
Rights	©2026 American Physical Society
Type	journal article
File Information	v5.pdf

Hokkaido University Collection of Scholarly and Academic Papers : HUSCAP

Microscopic formulation of the interacting boson-fermion model using the nuclear energy density functional

M. Homma[1] and K. Nomura[1,2,*]

[1] *Department of Physics, Hokkaido University, Sapporo 060-0810, Japan*
[2] *Nuclear Reaction Data Center, Hokkaido University, Sapporo 060-0810, Japan*

(Dated: May 28, 2026)

Microscopic modeling of low-energy spectroscopy in medium-heavy and heavy odd-A nuclei is an outstanding open problem in nuclear physics. We propose a novel spectra-generating collective model for odd-A nuclei constructed by means of the nuclear energy density functional theory and the interacting boson-fermion model. The bosonic Hamiltonian for an even-even nucleus, which is treated as a core, and the strength parameters for the interactions between the core and an odd nucleon are completely determined by using as microscopic inputs the potential energy curves and deformed single-particle spectra obtained from the self-consistent mean-field calculations. In applications to odd-A Eu, Sm, La, and Ba isotopes, we demonstrate the validity of the proposed method in reproducing reasonably the observed low-energy spectra and shape phase transitions in the general cases of the quadrupole collective states, that is, nearly spherical, strongly deformed, and γ-soft shapes, in the presence of an odd nucleon in a single-j orbit.

I. INTRODUCTION

Microscopic modeling of nuclei with odd numbers of nucleons remains a major challenge for nuclear theory. In even-even nuclei, which have even neutron N and proton Z numbers, to a good approximation nucleons are coupled pairwise with spin and parity $J = 0^+$, and this correlation determines, to a large extent, the nuclear structure in the vicinity of the ground state. As for the odd (denoted odd-A and odd-odd) nuclei, one should explicitly take into account unpaired nucleon degrees of freedom on the same footing as the collective degrees of freedom, and accurately model their couplings [1].

To simplify problems, it is often reasonable to represent an odd nucleus as a coupled system of an even-even nucleus as a core, which is dominated by collective degrees of freedom, and unpaired, single nucleons. Such a framework is provided by the interacting boson-fermion model (IBFM) [2, 3], in which the even-even core is represented as a many-body system of bosons in terms of the interacting boson model (IBM) [4, 5], and certain boson-fermion interactions are introduced. The IBFM was applied to descriptions of low-energy spectra and electromagnetic transition properties in odd-A nuclei in a wide range of the nuclear chart (see Refs. [3, 6] for a review), to analyze quantum phase transitions (QPTs) [7–12] and shape coexistence [13–15] in Bose-Fermi systems, to identify supersymmetric multiplets [7, 16–18], and to compute properties of nuclear decay processes including single β [19–24] and double β [25–27] decays.

The basic assumptions of the IBM are that correlated pairs of valence nucleons with $J^\pi = 0^+$ and 2^+ are associated with monopole, s, and quadrupole, d, bosons, respectively [5, 28, 29]. While the IBM has been successfully used for describing the low-energy collective structure in numerous numbers of nuclei, strength parameters of the boson Hamiltonian were determined to reproduce the experimental data. Microscopic formulation of the IBM, that is, derivation of the IBM Hamiltonian parameters from a more fundamental nuclear structure theory, was also made by various approaches; see, e.g., Refs. [29–31]. It was shown, in particular, that the IBM Hamiltonian for describing general quadrupole collective states, i.e., those associated with anharmonic vibrations [32], rotations [33], and γ-unstable rotations [34], was completely determined by using as microscopic inputs solutions of the self-consistent mean-field (SCMF) calculations that are performed within the nuclear energy density functional (EDF) framework [35–38]. This method was extensively used in nuclear structure studies describing nuclear spectroscopy related to, e.g., shape coexistence, octupole and hexadecapole shapes, in even-even systems (see the review [39] and references therein).

The microscopic foundation of the IBFM has also been investigated, e.g., in terms of the generalized seniority scheme of the nuclear shell model [40–43]. The EDF-based IBM, mentioned above, was extended to compute the spectroscopy of odd-A nuclei in Ref. [44]. In this method [44], the EDF-SCMF calculations yield the single-particle energies and occupation probabilities for an odd particle, which are used to construct the IBFM Hamiltonian. However, coupling constants for the boson-fermion interaction terms were left as free parameters, and were determined to reproduce to a certain accuracy the observed low-energy spectrum in each odd-A nucleus.

In the preceding work [45], we proposed a method to determine completely the IBFM Hamiltonian parameters by the EDF calculations. In the first step, the IBM Hamiltonian describing the even-even core nucleus was determined by employing the method of Refs. [31, 32], that is, the EDF-SCMF potential energy curve (PEC) along the quadrupole deformation β is mapped onto the expectation value of the IBM Hamiltonian in the condensate state of s and d bosons. In the second step, the

* nomura@sci.hokudai.ac.jp

boson-fermion strength parameters were derived so that the deformed single-particle spectra as functions of the axial deformation β in the intrinsic frame of the IBFM [3, 9, 46–48] were made to match those of the EDF-SCMF calculations for odd-A nuclei. In an illustrative application to axially deformed $^{149-159}$Eu isotopes, using the single-j (i.e., proton $1h_{11/2}$) orbit, this method was shown to be valid in reproducing excitation energies of low-energy negative-parity states without any adjustment of parameters to the experimental data. The calculation, in particular, correctly reproduced the change of the angular momentum I of the lowest-energy negative-parity states from $I = 11/2^-$ to $5/2^-$ near the neutron number $N = 90$, which can be considered to be an empirical signature of the shape QPTs in the odd-A systems [9, 48].

The results reported in Ref. [45] demonstrated the first successful case of the IBFM description with all the model parameters derived from the microscopic EDF inputs. From a practical point of view, the method developed in [45] is also considered to be an alternative EDF-based collective model able to provide predictions for low-energy spectroscopy in heavy odd-A nuclei. One might rather consider that a straightforward way to compute spectroscopic properties in the EDF model would be to project the mean-field solutions onto states with good symmetry quantum numbers, and to incorporate quantum fluctuation effects via configuration mixing by means of the generator coordinate method (GCM). The GCM was actually implemented in the EDF to study spectroscopy in odd-A nuclei, by fully taking into account the breaking of the time-reversal invariance and blocking effects [49–51]. However, practical applications of the projected EDF-GCM approach to a large number of odd-A and odd-odd nuclei are prohibitively demanding, and have been limited to light odd-A nuclei, e.g., Mg isotopes. In recent years advances have also been made in the *ab-initio* GCM descriptions of odd-A nuclei that are heavier than Mg (e.g., Ref. [52]). These present a promising microscopic approach to odd-A and odd-odd systems in medium to heavy mass regions.

Following up the initial study of Ref. [45], this article reports more systematic spectroscopic calculations for odd-A nuclei within the EDF-IBFM approach. The scope of the present paper is (i) to address the validity of the proposed method to describe, in addition to axially deformed systems, axially asymmetric nuclei that are expected to show pronounced γ softness; (ii) to show the robustness of the method in describing reasonably the odd-N and odd-Z systems, in which the odd nucleon i.e., neutron and proton, respectively, is the same as and different from the control parameter of the QPT (nucleon number) along the isotopic chain; and (iii) to develop a way of calculating the electromagnetic transition properties without any adjustment of the effective boson charges.

Nuclei we specifically consider in this study are axially deformed even-even $^{148-158}$Sm and odd-A $^{149-159}$Sm and $^{149-159}$Eu isotopes near the transitional region $N \approx 90$, and γ-soft even-even $^{128-134}$Ba and odd-A $^{129-135}$La and $^{127-133}$Ba isotopes in the mass $A \approx 130$ region. In Ref. [45], we discussed the shape transitions in odd-A Eu, which correspond to the manifest QPTs that are suggested to occur in the neighboring even-even Sm isotopes from the U(5) (associated with spherical vibrational shapes) to the SU(3) (strongly prolate deformed shapes) dynamical symmetries. The additions of the results for the Ba and La nuclei are used to investigate whether the proposed method works reasonably well in γ-soft systems, as in the case of the axially-deformed Eu and Sm. In the considered La and Ba region, in particular, another type of shape change between the U(5) and O(6) (representing γ-unstable shapes) dynamical symmetries is expected to occur [5, 53, 54].

The paper is organized as follows. In Sec. II, we introduce the procedure to derive the IBFM Hamiltonian parameters from the EDF-SCMF calculations. Section III provides calculated results, including the IBFM and HFB deformation energy curves, deformed single-particle energies, excitation energies for low-lying states, and electric quadrupole ($E2$) transitions. A summary is given and insights into possible future studies are provided in Sec. IV.

II. THEORETICAL FRAMEWORK

In the following, we use the simplest versions of the IBM and IBFM, in which like-neutron and like-proton bosons are not distinguished. The total number of bosons, denoted $N_{\rm B}$, equals the number of pairs of valence nucleons with respect to the nearest doubly magic nucleus. For the even-even $^{148-158}$Sm, $N_{\rm B} = 8, 9, \ldots, 13$, respectively, while for the even-even $^{128-134}$Ba, $N_{\rm B} = 8$, 7, 6 and 5, respectively, as the neutrons are hole-like. The IBFM Hamiltonian consists of the bosonic (IBM) Hamiltonian, $\hat{H}_{\rm B}$, single-nucleon Hamiltonian for an odd particle, $\hat{H}_{\rm F}$, and the particle-core interaction, $\hat{V}_{\rm BF}$ [3]:

$$\hat{H} = \hat{H}_{\rm B} + \hat{H}_{\rm F} + \hat{V}_{\rm BF}. \tag{1}$$

The IBM Hamiltonian of the form

$$\hat{H}_{\rm B} = \epsilon_d \hat{n}_d + \kappa \hat{Q} \cdot \hat{Q} \tag{2}$$

is employed, where the first term stands for the d-boson number operator, $\hat{n}_d = d^\dagger \cdot \tilde{d}$, with ϵ_d being the single-d-boson energy, and the second term the quadrupole-quadrupole boson interaction with the strength κ. The quadrupole operator is given as $\hat{Q} = s^\dagger \tilde{d} + d^\dagger \tilde{s} + \chi[d^\dagger \times \tilde{d}]^{(2)}$, with χ being another parameter. Note the notations $\tilde{s} = s$ and $\tilde{d}_\mu = (-1)^\mu d_{-\mu}$.

As in the previous work [45], we shall consider single-j problems, that is, for the single-particle space we take the proton $1h_{11/2}$ and neutron $1i_{13/2}$ orbits for the odd-A Eu and Sm, respectively, and the neutron and proton $1h_{11/2}$ orbits for the odd-A Ba and La, respectively. The

spectroscopic properties in the odd-A nuclei discussed in the following, therefore, all arise from the configurations of the unique-parity orbit coupled to the even-even boson core. Since the scope of this study includes addressing the validity of the procedure in a systematic way in different mass regions, the assumption of taking into account only a single-j orbit for the odd particle would not lose much generality. The extension to the multiple-j cases can be straightforward, but is also beyond the scope of the present study.

In the single-j case, the Hamiltonian $\hat{H}_{\rm F}$ in (1) is given simply as

$$\hat{H}_{\rm F} = -\epsilon_j \sqrt{2j+1}[a_j^\dagger \times \tilde{a}_j]^{(0)} \equiv \epsilon_j \hat{n}_j \ , \tag{3}$$

where $a_j^\dagger$ and $\tilde{a}_{j,m} \equiv (-1)^{j-m} a_{j,-m}$ stand for the particle creation and annihilation operators, respectively, and ϵ_j is the single-particle energy.

The boson-fermion interaction, $\hat{V}_{\rm BF}$, can be expressed in the following compact form, consisting only of three essential interactions that are sufficient for numerical studies [3]:

$$\hat{V}_{\rm BF} = \Gamma \hat{V}_{\rm dyn} + \Lambda \hat{V}_{\rm exc} + A \hat{V}_{\rm mon} \ , \tag{4}$$

where the first, second, and third terms are, respectively, so-called dynamical (quadrupole) term, representing direct boson-fermion interactions, the exchange term, which reflects that bosons are made of nucleon pairs, and the monopole interaction. They are expressed as

$$\hat{V}_{\rm dyn} = \hat{Q} \cdot [a_j^\dagger \times \tilde{a}_j]^{(2)} \tag{5}$$

$$\hat{V}_{\rm exc} =: [[d^\dagger \times \tilde{a}_j]^{(j)} \times [\tilde{d} \times a_j^\dagger]^{(j)}]^{(0)} : \tag{6}$$

$$\hat{V}_{\rm mon} = \hat{n}_d \hat{n}_j \ . \tag{7}$$

The notation $: [\cdots] :$ in Eq. (6) denotes normal ordering. In the generalized seniority scheme, the strength parameters Γ, Λ, and A in Eq. (4) are further simplified to be of the forms [40]

$$\Gamma = \Gamma_0 \gamma_{jj} \tag{8}$$

$$\Lambda = -2\Lambda_0 \sqrt{\frac{5}{2j+1}} \beta_{jj}^2 \tag{9}$$

$$A = A_0 \ , \tag{10}$$

where $\gamma_{jj} = (u_j^2 - v_j^2) Q_{jj}$ and $\beta_{jj} = 2u_j v_j Q_{jj}$, with $Q_{jj} = \langle j || Y^{(2)} || j \rangle$ being the matrix element of the quadrupole operator in the single-particle basis. v_j and u_j are the occupation and unoccupation amplitudes for the orbital j, satisfying the relation $u_j^2 + v_j^2 = 1$. Γ_0, Λ_0, and A_0 are strength parameters.

To associate with the intrinsic properties generated by the SCMF method, the geometry of the IBFM Hamiltonian (1) is formulated using the following basis:

$$|N_{\rm B}; \bar{\beta}, \bar{\gamma}; j, m\rangle = |N_{\rm B}; \bar{\beta}, \bar{\gamma}\rangle \otimes |j, m\rangle \ . \tag{11}$$

$|j, m\rangle$ stands for the single-particle basis for an odd nucleon, $|j, m\rangle = a_{j,m}^\dagger |0\rangle$. $|N_{\rm B}; \bar{\beta}, \bar{\gamma}\rangle$ denotes the coherent state [55] of s and d bosons, given as

$$|N_{\rm B}; \bar{\beta}, \bar{\gamma}\rangle = (N_{\rm B}!)^{-1/2} (b_c^\dagger)^{N_{\rm B}} |0\rangle \ , \tag{12}$$

with

$$b_c^\dagger = (1+\bar{\beta}^2)^{-1/2} \left[s^\dagger + d_0^\dagger \bar{\beta} \cos\bar{\gamma} + \frac{1}{\sqrt{2}} (d_{+2}^\dagger + d_{-2}^\dagger) \bar{\beta} \sin\bar{\gamma} \right] . \tag{13}$$

$\bar{\beta}$ and $\bar{\gamma}$ are boson analogs of the axial quadrupole deformation β and triaxiality γ [1], respectively. $|0\rangle$ represents the inert core or a doubly magic nucleus, i.e., ^{132}Sn. For simplicity, we assume that the bosonic deformation $\bar{\beta}$ is proportional to the fermionic deformation β [31, 55], and that the bosonic triaxiality $\bar{\gamma}$ is the same angle variable as the fermionic counterpart γ:

$$\bar{\beta} = C_{\rm B} \beta \tag{14}$$

$$\bar{\gamma} = \gamma \tag{15}$$

with $C_{\rm B}$ being a constant of proportionality. The factor $C_{\rm B}$ in (14) is introduced to take into account the difference in model space between the IBM and SCMF model: the former comprises valence nucleons in a given model space, while in the latter all constituent nucleons are considered in a much larger fermionic configuration space. By taking the expectation value of the IBFM Hamiltonian (1) in the basis (11), the energy surface for an odd-A nucleus is obtained in a matrix form [46]. In this study, we assume axial symmetry ($\gamma = 0°$), and hereafter omit the argument γ. This assumption makes the energy surface matrix diagonal, and each diagonal element, given by

$$E_K = E_{\rm B}(\beta; \xi) + \lambda_K(\beta; \eta) \ , \tag{16}$$

corresponds to the energy of the state with the projection $m = K$. The entire energy surface for the IBFM is calculated as the sum of the bosonic energy surface, $E_{\rm B}(\beta; \xi)$, and the single-particle energy, $\lambda_K(\beta; \eta)$. Here ξ and η denote sets of the parameters involved in $E_{\rm B}$ and λ_K, respectively:

$$\xi = \{\epsilon_d, \kappa, \chi, C_{\rm B}\} \ , \quad \eta = \{\Gamma_0, \Lambda_0, A_0\} \ . \tag{17}$$

Each term in (16) is calculated as [3, 46]

$$\begin{aligned} E_{\rm B}(\beta; \xi) &= \langle N_{\rm B}; \bar{\beta} | \hat{H}_{\rm B} | N_{\rm B}; \bar{\beta} \rangle \\ &= \frac{N_{\rm B}}{1+\bar{\beta}^2} \left\{ 5\kappa + \left[\epsilon_d + \kappa(1+\chi^2) \right] \bar{\beta}^2 \right\} \\ &\quad + \kappa \frac{N_{\rm B}(N_{\rm B}-1)\bar{\beta}^2}{(1+\bar{\beta}^2)^2} \left(2 - \chi \sqrt{\frac{2}{7}} \bar{\beta} \right)^2 \end{aligned} \tag{18}$$

$$\begin{aligned} \lambda_K(\beta; \eta) &= \langle N_{\rm B}; \bar{\beta}; j, m | (\hat{H}_{\rm F} + \hat{V}_{\rm BF}) | N_{\rm B}; \bar{\beta}; j, m \rangle \\ &= \epsilon_j + A \frac{N_{\rm B} \bar{\beta}^2}{1+\bar{\beta}^2} + \frac{N_{\rm B} \bar{\beta}}{1+\bar{\beta}^2} \left[3K^2 - j(j-1) \right] P_j \\ &\quad \times \left\{ \Gamma \left(\chi \sqrt{\frac{2}{7}} \bar{\beta} - 2 \right) - \Lambda P_j \sqrt{2j+1} [3K^2 - j(j+1)] \bar{\beta} \right\}, \end{aligned} \tag{19}$$

where $P_j = [(2j-1)j(2j+1)(j+1)(2j+3)]^{-1/2}$. We assume that χ in Eq. (19) is the same as that in Eq. (18).

The model parameters, ξ for the IBM cores and η for the boson-fermion interaction, are determined in the following way [45].

1. In the first step, we perform the constrained SCMF calculations to obtain the one-dimensional PEC for even-even core nuclei and deformed single-particle energies for the neighboring odd-A nuclei. The constraints to the SCMF calculations are those on the mass quadrupole moment Q_{20}, which is related to the geometrical deformation β. In this study, we adopt the Hartree-Fock-Bogoliubov (HFB) method using the SkM* interaction [56] of the Skyrme EDF [57]. The SCMF calculations are carried out by using the computer program HFBTHO (v4.0) [58].

2. Next, we determine the parameters for the boson-core Hamiltonian $\hat{H}_{\rm B}$ by mapping the HFB PEC obtained in the previous step onto the IBM energy curve (18):

$$E_{\rm B}(\beta;\xi) \approx E_{\rm HFB}(\beta)\ . \tag{20}$$

   In this procedure, the set of the IBM parameters, ξ, are calibrated so that basic characteristics of the bosonic energy curves in the vicinity of the equilibrium minimum, such as the depth of the potential, and curvature up to a few MeVs from the minimum, should be made similar to those of the HFB PEC. The scale factor $C_{\rm B}$ (14) is determined so that IBM PEC reproduces the location of the energy minimum in the HFB PEC.

3. In the final step, the strength parameters, η, for the boson-fermion interaction, $\hat{V}_{\rm BF}$ (4), are fixed so that the single-particle energies of the IBFM, $\lambda_K(\beta;\eta)$ (19), should reproduce for each K value the HFB counterparts, $\epsilon_K(\beta)$, near the equilibrium minimum:

$$\lambda_K(\beta_e;\eta) \approx \epsilon_K(\beta_e)\ . \tag{21}$$

   By this procedure, the behaviors of the IBFM deformed single-particle spectra are made to resemble those of the HFB ones within the range of the deformation $0 \leqslant \beta \leqslant \beta_e$, where β_e is the deformation corresponding to the minimum in the HFB PEC for an odd-A nucleus. In the HFB calculations the blocking effects are taken into account at each deformation β and for all possible single-particle orbits [58]. The v_j and u_j amplitudes, which enter the formulas (8) and (9), are obtained from the Skyrme-HFB calculations performed at the spherical configuration, i.e., those that are constrained to zero quadrupole deformation, as was done in Ref. [44].

The IBFM Hamiltonian (1) with all the parameters fixed by the aforementioned procedure is numerically diagonalized in the basis $|L\otimes j; I\rangle$ [59], where L denotes the angular momentum of the boson system and I the total angular momentum of the odd-A system. This gives rise to energy levels, and wave functions to compute electromagnetic transition properties.

III. RESULTS

A. Potential energy curves of even-even nuclei

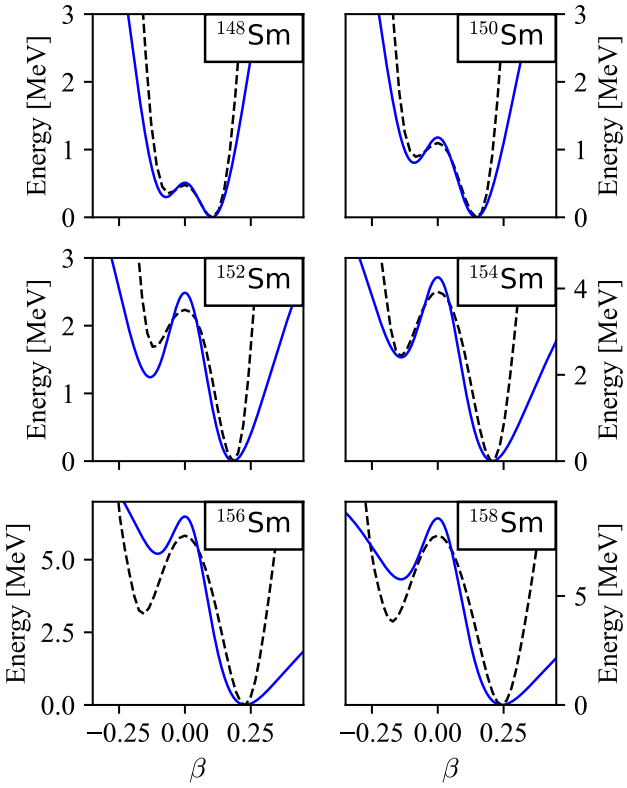

FIG. 1. Potential energy curves along the axial quadrupole deformation β for the even-even nuclei $^{148-158}$Sm calculated within the Skyrme-HFB (dashed curves) and IBM (solid curves).

In Figs. 1 and 2, the IBM PECs for the even-even-core nuclei are shown, together with the original Skyrme-HFB PECs. The HFB PECs for the Sm isotopes show patterns of an empirically suggested shape phase transition, that is, a transition from a weakly deformed prolate shape with an equilibrium minimum $\beta_e = 0.10$ in ^{148}Sm to a strongly deformed prolate shape near ^{154}Sm. The IBM PECs appear to reproduce overall behaviors of the Skyrme-HFB PECs. However, as the deformation becomes larger, $\beta > 0.3$, the IBM PEC becomes flat compared with the HFB one. This deviation reflects the difference in the size of the model space and degrees of freedom between the IBM and HFB, as pointed out in Sec. II. In the HFB configurations of the large defor-

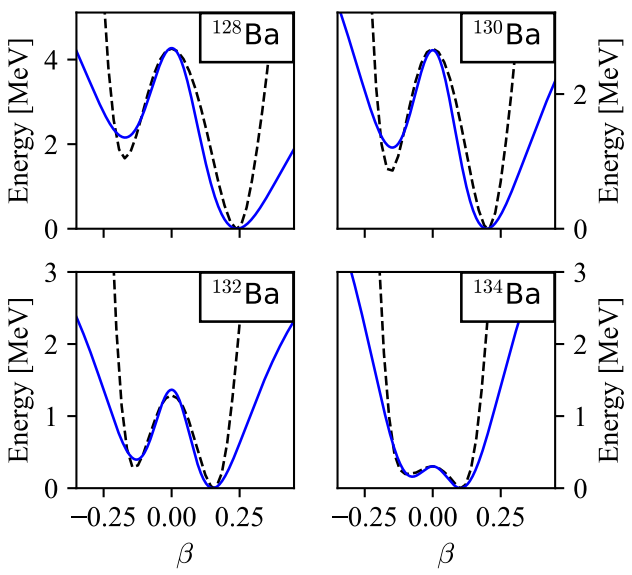

FIG. 2. Same as the caption to Fig. 1, but for $^{128-134}$Ba.

mations, $\beta \gg \beta_e$, noncollective, quasiparticle excitations begin to play a part, but these modes of excitations are outside of the standard IBM model space. This is the reason why the mapping is made to reproduce features of the HFB PEC in the vicinity of the equilibrium minimum. One also notices a discrepancy between the HFB and IBM curves near the oblate saddle points in heavier Sm, most notably, in ^{156}Sm and ^{158}Sm. This arises because the PEC mapping is made for the energy range of up to 2-3 MeV from the equilibrium minimum. In the above two nuclei, in which the potential is particularly deep, the IBM reasonably reproduces the behavior of the HFB PEC on the prolate side, but this is not the case with the oblate side.

The HFB PECs shown in Fig. 2 suggest a prolate shape in ^{128}Ba and ^{130}Ba. The energy difference between the prolate equilibrium minimum at $\beta_e \approx 0.2$ and the oblate saddle point becomes smaller as one approaches ^{134}Ba. This implies that the potential becomes soft in γ deformation, and thus indicates a prolate-to-γ-soft shape transition. It should be noted that, while the present study is restricted to axially symmetric deformation, the triaxiality would have potential impacts on the IBM parameters and resulting low-lying states. In fact, earlier SCMF calculations of the triaxial quadrupole deformation energy surfaces that are based on the nonrelativistic Skyrme (e.g., [32]), Gogny (e.g., [60, 61]), and relativistic (e.g., [62, 63]) EDFs suggested a shallow triaxial minimum with a nonzero γ deformation in the nuclei in the $A \approx 130$ Ba region. The γ softness is here accounted for in the IBM by the value of the parameter χ that is small in magnitude, since in the γ-unstable O(6) limit of the IBM this parameter is supposed to be zero. To describe more quantitatively possible effects of the triaxiality on low-lying states, cubic (three-body) boson terms would need to be included in the IBM Hamiltonian, with their strength parameters being obtained from mapping of the triaxial HFB energy surfaces [34]. This requires a major extension of the method, but would be an interesting future work.

B. Deformed single-particle spectra

Figure 3 depicts the IBFM and Skyrme-HFB deformed single-particle energies for the odd-Z nuclei, $^{149-159}$Eu, originating from the proton $1h_{11/2}$ spherical orbit, and those for the odd-N nuclei, $^{149-159}$Sm, originating from the neutron $1i_{13/2}$ orbit. It is seen that the IBFM single-particle orbits $\lambda_K(\beta;\eta)$ reproduce reasonably well the HFB counterparts within the ranges $0 \leqslant \beta \leqslant \beta_e$.

One may also notice that, for very large quadrupole deformations ($\beta \gg \beta_e$), the IBFM single-particle energies become flat, whereas those from the HFB calculations in general exhibit much more significant changes with β. This difference arises from the limited IBFM model space as compared with that of the HFB, and we have seen in Fig. 1 a similar discrepancy when comparing the HFB and IBM PECs. As pointed out earlier, the SCMF configurations at the very large deformations are beyond the model spaces of the standard IBM and IBFM, hence the comparisons of the IBFM with the HFB single-particle orbits in the region $\beta \gg \beta_e$ would not make much sense, but should be made within the range $0 \leqslant \beta \leqslant \beta_e$.

The relation (21) used to obtain the set of the IBFM parameters, η, turns out to be a good approximation for those odd-A nuclei with $N \leqslant 89$, which are moderately deformed, $\beta_e \approx 0.15$. For these nuclei, the IBFM single-particle energies reasonably reproduce the HFB ones in the range $0 \leqslant \beta \leqslant \beta_e$. However, for more deformed odd-A nuclei with $N \geqslant 90$, which typically exhibit a larger β_e value, $\beta_e \geqslant 0.2$, the relation of (21) does not appear to hold, because the behaviors of the IBFM energies, $\lambda_K(\beta;\eta)$, differ significantly from those of the HFB ones near the configurations $\beta \approx \beta_e$. The reasons for this to occur are, as mentioned, the limited size of and degrees of freedom in the IBFM configuration space, and also the fact that the analytical form of the formula (19) may be of too simplified a form. To take these into account, in Ref. [45] we assumed that, specifically for well deformed odd-A Eu nuclei typically exhibiting $\beta_e \geqslant 0.2$, the scale factor $C_{\rm B}$ for the β deformation for the bosonic part, $E_{\rm B}(\beta;\xi)$ (18), could be different from that in the boson-fermion coupling part, $\lambda_K(\beta;\eta)$ (19), and we replaced $C_{\rm B}$ in the formula (19) with a new parameter $C_{\rm BF}$. We here apply this procedure to the odd-A Sm nuclei as well, and consider the following formula for the deformed odd-A Eu nuclei with $N \geqslant 90$ and Sm with $N \geqslant 91$:

$$E_K(\beta) = E_{\rm B}(\beta;\xi) + \lambda_K(\beta;\eta') \ , \qquad (22)$$

where η' denotes the set of parameters, $\eta' = \{A_0, \Gamma_0, \Lambda_0, C_{\rm BF}\}$. For those Eu and Sm isotopes with $N \leqslant 88$ and $N \leqslant 90$, respectively, common $C_{\rm B}$ values

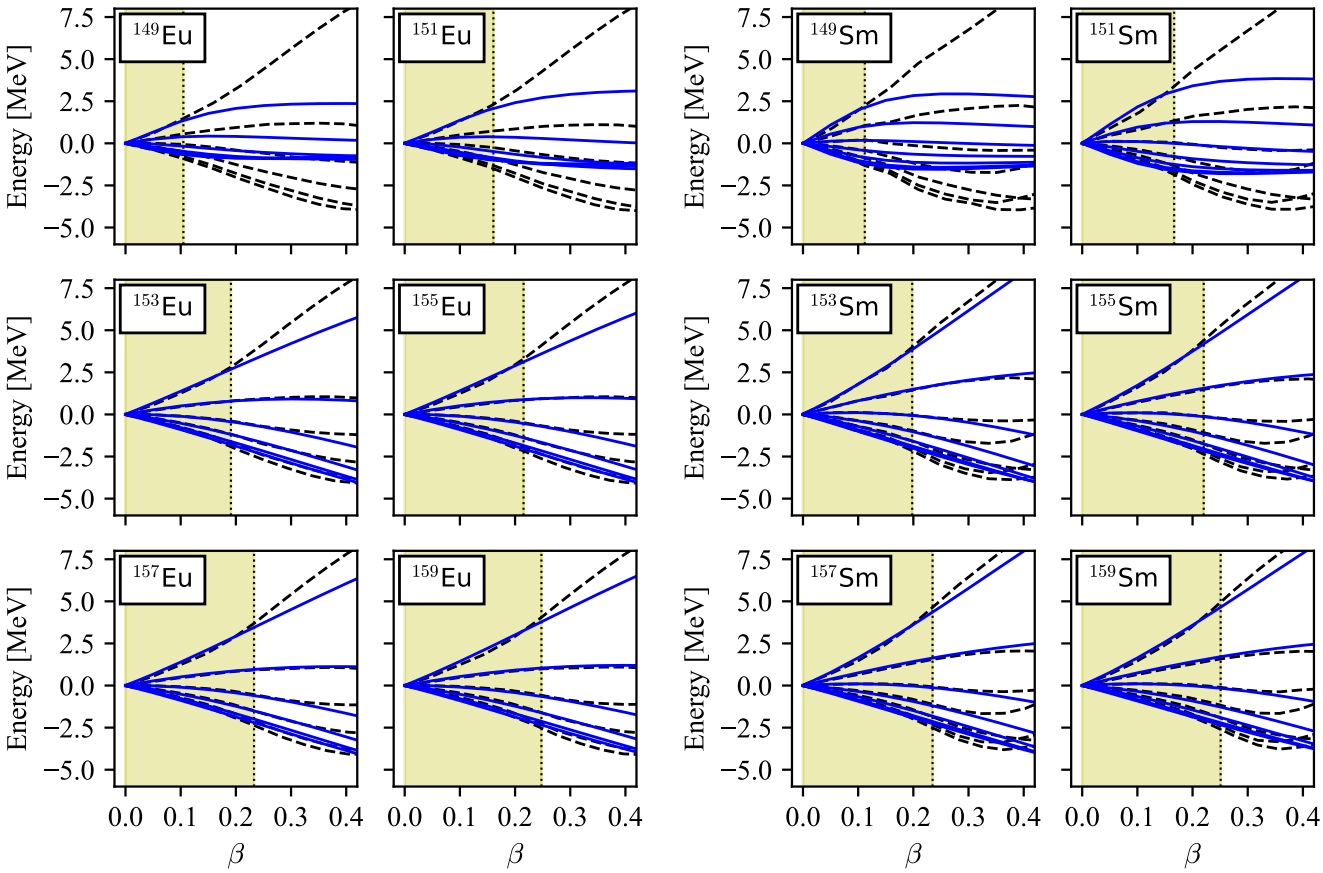

FIG. 3. Deformed single-particle spectra calculated for the odd-Z nuclei $^{149-159}$Eu and odd-N nuclei $^{149-159}$Sm within the IBFM (solid curves), Eq. (19), and the HFB-SCMF method (dashed curves). Yellow-shaded areas indicate the range of the deformation β, within which the IBFM single-particle spectra are matched to those of the HFB. The IBM single-particle spectra corresponding to different values of the K quantum number, $K = 1/2$, 3/2, 5/2, 7/2, 9/2, and 11/2 ($K = 1/2$, 3/2, 5/2, 7/2, 9/2, 11/2, and 13/2), in increasing order in energy, are compared with the HFB ones, which are labeled by the asymptotic quantum numbers $K[Nn_z m_l]$ that are equal to 1/2[550], 3/2[541], 5/2[532], 7/2[523], 9/2[514], 11/2[505] (1/2[660], 3/2[651], 5/2[642], 7/2[633], 9/2[624], 11/2[615], 13/2[606]), respectively, for the odd-A Eu (Sm) isotopes

are considered for both the boson, $E_{\rm B}(\beta;\xi)$, and boson-fermion, $\lambda_K(\beta;\eta)$, parts, i.e., $C_{\rm B} = C_{\rm BF}$. Using different scale factors, i.e., $C_{\rm B}$ for boson part and $C_{\rm BF}$ for boson-fermion interaction part, for those nuclei with $N \geqslant 90$, effectively takes into account the fact that, while the single-particle orbit couples weakly to the even-even core that is close to nearly spherical vibrational limit, in strongly deformed systems the particle-core coupling is expected to be stronger. Specifically, the formula (22) is used in those cases in which the HFB energy curves exhibit a substantially steep (> 2 MeV) potential with a distinct axial prolate minimum typically found at $\beta_e \geqslant 0.2$, such as the even-even Sm nuclei with $A \geqslant 152$ (see Fig. 1).

Figure 4 shows the HFB and IBFM deformed single-particle spectra for $^{129-135}$La and $^{127-133}$Ba, which originate from the proton and neutron $1h_{11/2}$ spherical orbits, respectively. One can observe that the IBFM reasonably reproduces the HFB single-particle energies within the ranges $0 \leqslant \beta \leqslant \beta_e$. For these odd-$A$ nuclei, the formula (16) is consistently used for all the La and Ba isotopes considered. This is mainly because the quadrupole correlations in these systems are, in general, not as pronounced as in the case of the Eu and Sm nuclei. That is, even though a large quadrupole deformation, $\beta_e \approx 0.2$, is suggested for some of these odd-A La and Ba nuclei, as compared with those for the Sm and Eu nuclei, the HFB PECs for the corresponding even-even Ba nuclei exhibit potentials that are rather shallow and are expected to be soft in γ deformation, as the energy difference between the prolate equilibrium minimum and the oblate saddle point is more or less small.

C. Derived parameters

The derived IBFM parameters for all the considered odd-A isotopes are presented in Figs. 5 and 6. Table I summarizes the occupation probabilities for the spherical

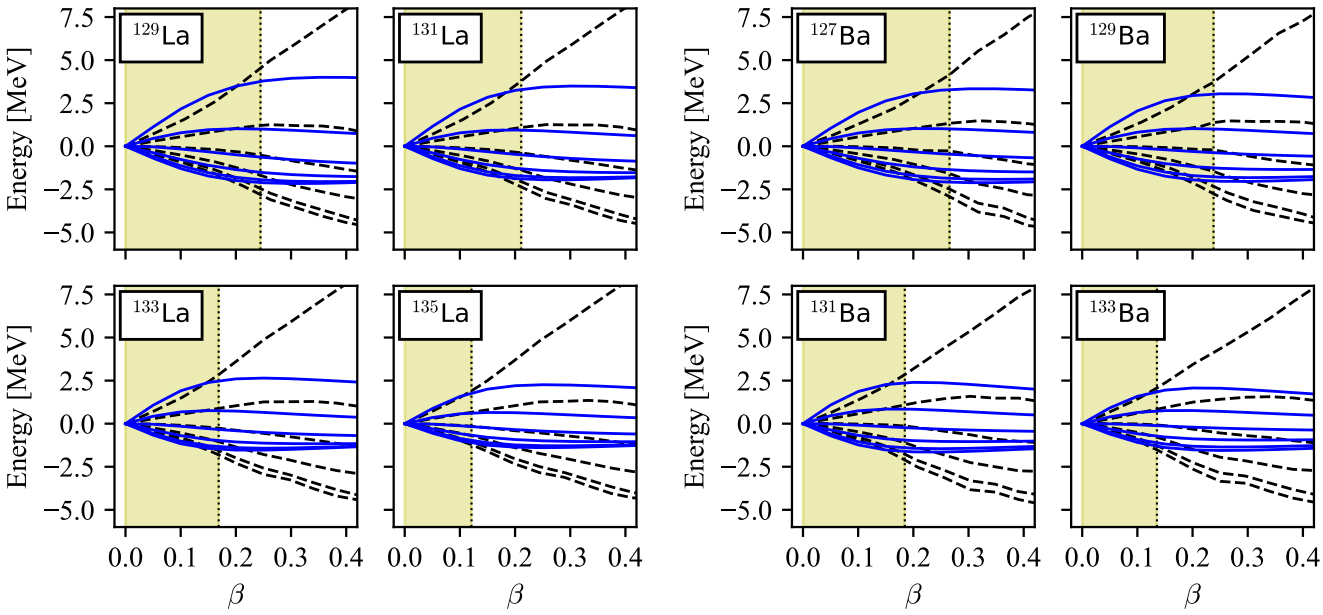

FIG. 4. Same as the caption to Fig. 3, but for the odd-Z $^{129-135}$La and odd-N $^{127-133}$Ba.

single-particle orbits. The parameters for the even-even Sm and odd-A Eu, plotted in Figs. 5(a) –5(h), are taken from Ref. [45]. Note that the boson-fermion interaction strengths that are shown in Figs. 1(e)–1(g) of [45] with the notations Γ, Λ, and A in the vertical axes correspond to the parameters denoted Γ_0, Λ_0, and A_0 in the expressions (8) –(10). These differences in notations do not at all affect the final results and conclusions given in the following, and the calculations in the present work and in Ref. [45] are all consistent.

TABLE I. Occupation probabilities v_j^2 for the odd-A nuclei obtained from the HFB calculations constrained to the deformation $\beta = 0$. The single-particle orbits used in this study are the proton $1h_{11/2}$ for the Eu and La isotopes, neutron $1i_{13/2}$ for the odd-A Sm and neutron $1h_{11/2}$ for the odd-A Ba.

Nuclei	$v^2_{\pi h_{11/2}}$	Nucleus	$v^2_{\nu i_{13/2}}$	Nucleus	$v^2_{\pi h_{11/2}}$	Nucleus	$v^2_{\nu h_{11/2}}$
^{149}Eu	0.177	^{149}Sm	0.011	^{129}La	0.081	^{127}Ba	0.376
^{151}Eu	0.167	^{151}Sm	0.020	^{131}La	0.079	^{129}Ba	0.479
^{153}Eu	0.159	^{153}Sm	0.072	^{133}La	0.078	^{131}Ba	0.560
^{155}Eu	0.154	^{155}Sm	0.083	^{135}La	0.077	^{133}Ba	0.667
^{157}Eu	0.150	^{157}Sm	0.138				
^{159}Eu	0.145	^{159}Sm	0.192				

We show from Figs. 5(a) to 5(d) the IBM parameters for the even-even Sm isotopes derived from the PEC-mapping procedure. We can observe gradual evolution of these parameters as functions of N, confirming the empirical evidence that the quadrupole collectivity becomes stronger with nucleon numbers in rare-earth nuclei. A notable change is found in the systematic of the derived parameter χ, shown in Fig. 5(c), which rapidly decreases from $N = 92$ to 94 to a value approximately close to the SU(3) limit of the IBM, $\chi = -\sqrt{7}/2 \approx -1.32$ [5]. This irregularity at $N = 94$ may have arisen from numerical fitting, and thus appears to be rather accidental. Similar local behaviors at $N = 94$ are also obtained in the parameters κ and $C_{\rm B}$. The present values of the IBM parameters are compared with those from earlier studies using the generalized seniority scheme [40] and with those from the previous mapped IBM calculations of Ref. [10], which employed the relativistic EDF calculations to determine the IBM Hamiltonian and v_j^2 values. The present ϵ_d values are consistent with the ones in Refs. [10, 40] in systematics, and the derived χ parameters in this study are similar to those in Ref. [10]. However, the κ strengths adopted here are significantly different from the previous two IBM studies. This parameter seems to be most sensitive to the microscopic inputs from the fermionic calculations: the κ value of [44] was derived with the inputs from the relativistic EDF calculations, and the one in [40] was obtained using the schematic (surface delta) shell model interaction.

In Figs. 5(e)– 5(h), we show the IBFM parameters for $^{149-159}$Eu, which are derived by using the formulas (16) and (22). We can see that all these parameters display a drastic change from $N = 88$ to 90. The abrupt change of the parameters reflects evolution of nuclear structure in the odd-A systems, which takes place along with that in the neighboring even-even Sm cores. What is worth a remark is that the scale factor $C_{\rm BF}$ for deformed odd-A Eu nuclei with $N \geqslant 90$ is chosen to be unity, which means that the IBFM single-particle energies are dictated by the same amount of deformation as the geometrical one

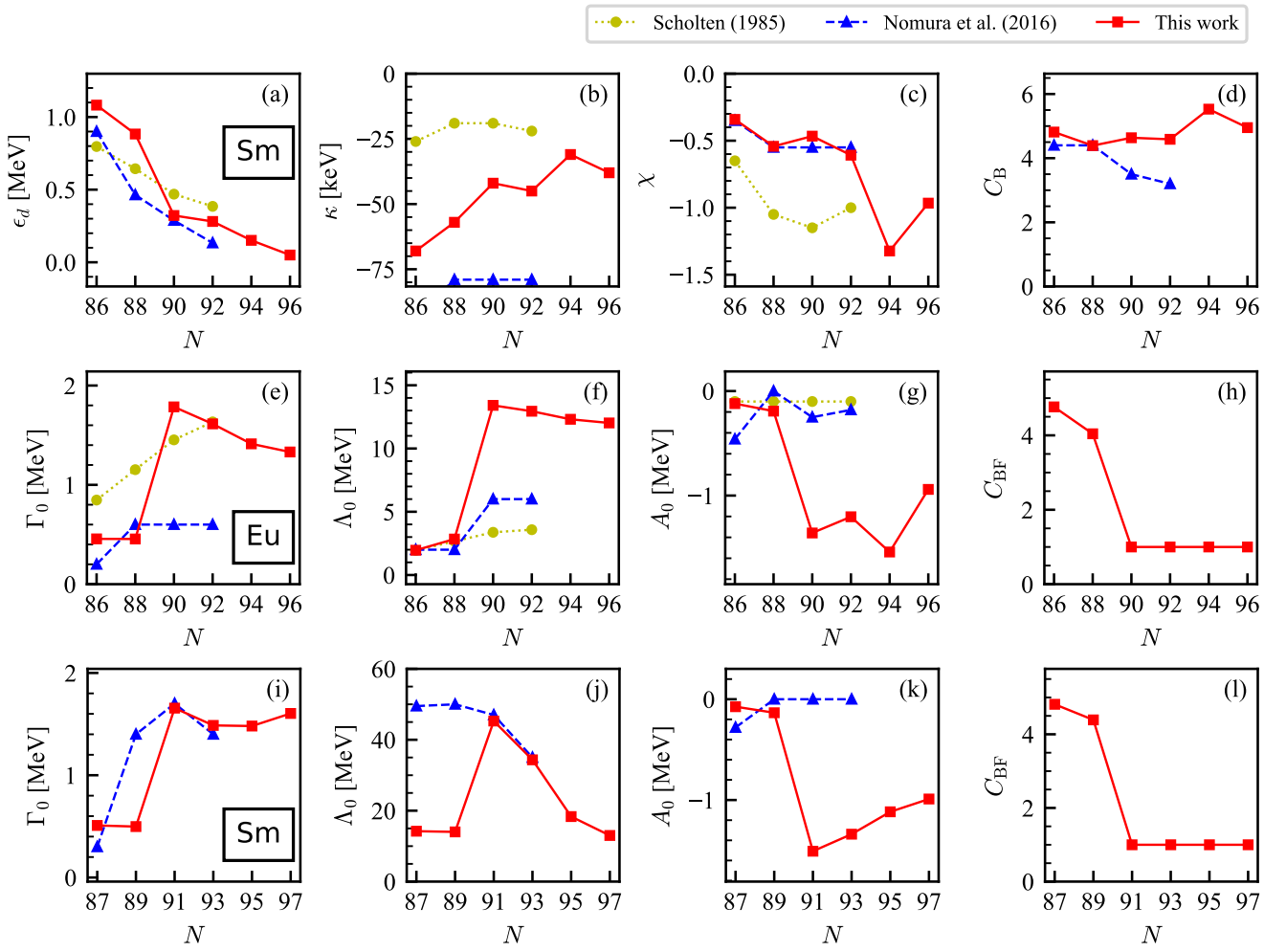

FIG. 5. Derived IBM parameters for the even-even $^{148-158}$Sm [(a)–(d)], boson-fermion interaction strengths and $C_{\rm BF}$ values for the odd-A $^{149-159}$Eu [(e)–(h)] and $^{149-159}$Sm [(i)–(l)] (represented by the squares connected by the solid curves). The values of the parameters denoted "This work" in (a)–(h) are adopted from Ref. [45]. Also in (a)–(c), in (e)–(g), and in (i)–(k), the IBM and IBFM parameters used in Ref. [10] ["Nomura *et al.* (2016)," represented by the solid triangles] and Ref. [40] ["Scholten (1985)," solid circles] are shown.

in deformed nuclei. Furthermore, the present IBFM parameters, in most cases, differ from those used in the previous IBFM calculations of Refs. [40, 44]. For instance, the present Γ_0 and Λ_0 strengths are larger than those in these earlier studies, and the present A_0 strength exhibits a stronger N dependence.

The derived IBFM parameters for the odd-A Sm nuclei are depicted in Figs. 5(i)– 5(l). As in the case of the odd-A Eu, there appear discontinuous changes of the parameters from $N = 89$ to 91, near which the even-even Sm undergo a rapid shape phase transition. We also compare our results with the IBFM parameters obtained in the previous calculations of Ref. [10]. The present Γ_0 values are of the same order of magnitude as those in [10], except for the nucleus ^{151}Sm. In the present study, much smaller Λ_0 values are obtained for the nuclei with $N \leqslant 89$ than those in [10], but those Λ_0 values derived here for ^{153}Sm and ^{155}Sm are consistent with those in [10]. The present monopole strengths A_0 are generally larger in magnitude than the ones in [10], in which $A_0 = 0$ MeV for $N \geqslant 89$. Among the odd-A systems under investigation, exchange strengths chosen in the present work and in Ref. [10] for the odd-A Sm turn out to be particularly large, $\Lambda_0 > 10$ MeV. This is due to the small $v^2_{\nu i_{13/2}}$ values (see Table I), which according to the formula (9) lead to vanishing $\beta_{i_{13/2},i_{13/2}}$ values.

Figures 6(a)– 6(d) show the IBM parameters for the even-even $^{128-134}$Ba nuclei, obtained from the PEC-mapping procedure. These IBM parameters exhibit a more gradual evolution than those for the Sm isotopes. This is consistent with the empirical finding that the shape phase transition occurs moderately in the mass $A \approx 130$ region. In the γ-soft systems, the potential

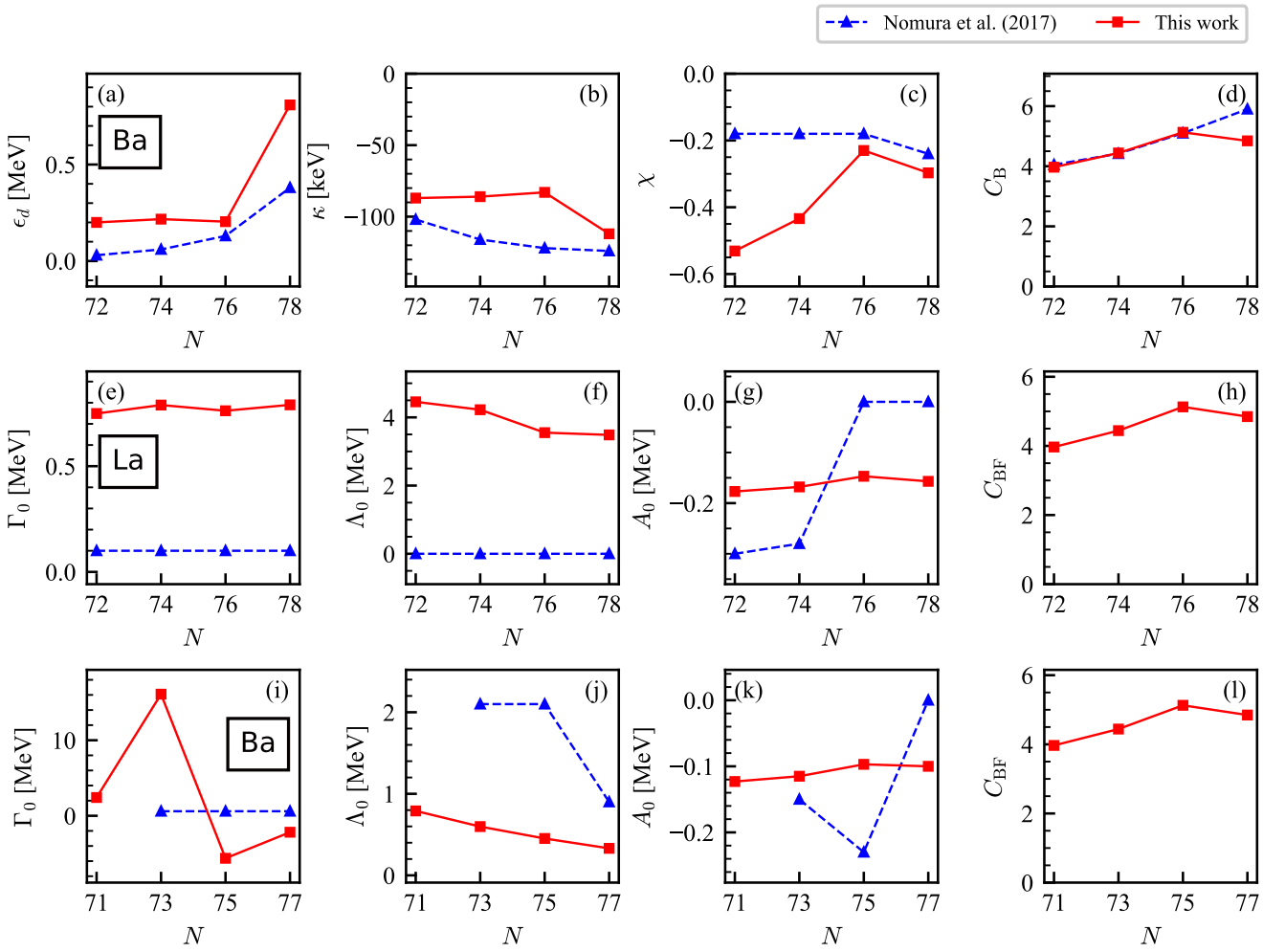

FIG. 6. Similar to the caption to Fig. 5, but for those parameters obtained in the present work for even-even $^{128-134}$Ba [(a)–(d)], odd-Z $^{129-135}$La [(e)–(h)], and odd-N $^{127-133}$Ba [(i)–(l)]. The parameters used in the previous IBFM study of Ref. [63] are also shown ["Nomura *et al.* (2017)," triangles]

energy surface is approximately independent of the γ deformation, which is characteristic of the O(6) dynamical symmetry of the IBM, and the χ parameter in the quadrupole operator is supposed to be close to zero. One can indeed see in Fig. 6(c) that the absolute value of χ for each Ba isotope is generally $|\chi| < 0.5$, which is much smaller than the SU(3) limit, $|\chi| = \sqrt{7}/2 \approx 1.32$.

One should also notice in Figs. 6(a) and 6(b) abrupt changes of the derived energy ϵ_d and strength κ from $N = 76$ to 78. These behaviors also reflect the shape phase transition in the Ba isotopes chain. As one can see in Fig. 2 the potential valley in the PEC for ^{134}Ba is much shallower than that of the neighboring ^{132}Ba. In terms of the IBM, the shape transition is expected to occur in the Ba isotopes from the O(6) to U(5) limits near $N = 78$, and the nuclei ^{132}Ba and ^{134}Ba have been considered to be close to the O(6) limit. The nucleus ^{134}Ba was also identified [54] as an empirical realization of the E(5) critical-point symmetry [53] of the O(6)-U(5) QPT.

The IBM parameters obtained from the mapping from the relativistic SCMF calculations in Ref. [63] are given in Figs. 6(a) –6(d). They show similar systematic to those of the present parameter values. However, the values of the χ parameter for ^{128}Ba and ^{130}Ba in the present work are larger in magnitude than those used in [63]. The difference indicates that the Skyrme-HFB PEC is steeper in γ deformation than the relativistic one. This conclusion may be, however, altered if the triaxial degree freedom is taken into account in the Skyrme HFB calculation.

The IBFM Hamiltonian parameters for the odd-A $^{129-135}$La are shown in Figs. 6(e) –6(h). Most of the derived parameters do not show any strong dependence on N. These behaviors conform to the gradual shape evolution in the neighboring even-even Ba. Figures 6(e) –6(g) give the boson-fermion strengths of Ref. [63], which

were fitted to experiment. The Γ_0 and Λ_0 strengths of [63] are much smaller than those derived in the present work. The derived Λ_0, A_0, and $C_{\rm BF}$ values for the odd-A $^{127-133}$Ba isotopes, shown Figs. 6(i) –6(l), exhibit a gradual change with N, but the adopted Γ_0 value for ^{129}Ba appears to be anomalously large. This is due to the HFB occupation probability $v^2_{\nu h_{11/2}} = 0.479$ for this nucleus (see Table I), which is rather close to 0.5. With $v^2_{\nu h_{11/2}} \approx 0.5$, meaning that the $1h_{11/2}$ neutron orbit is approximately half filled, the coefficient $\beta_{h_{11/2},h_{11/2}}$ in (9) becomes so negligibly small that the large Γ_0 value is required. The strength parameters Γ_0, Λ_0, and A_0 obtained in Ref. [63] exhibit behaviors that in general differ from those in the present work. It is, however, also noted that in Ref. [63] for the odd-N Ba nucleus with mass A the corresponding boson core was taken to be the even-even Ba nucleus with mass $A-1$, which means that the boson core for the odd-N Ba nucleus in Ref. [63] was taken to be different from that in the present calculation.

D. Potential energy curves in odd-A systems

We show in Fig. 7 the HFB and IBFM PECs (22) for the odd-A nuclei $^{149-159}$Eu and $^{149-159}$Sm, corresponding to the different values of the K quantum number, i.e., $K = 1/2,\ 3/2,\ \ldots,\ 11/2$ and $K = 1/2,\ 3/2,\ \ldots,\ 13/2$, respectively. Because the IBFM PECs should be obtained for each K value, it is not possible to compare them directly with the HFB PEC. Nevertheless, most of the IBFM PECs with different K values show similar behavior to the HFB PEC: the potential becomes deeper as N increases, and its minimum shifts from $\beta_e = 0.10$ (0.11) to 0.25 (0.25) in Eu (Sm) isotopes. We can infer from these behaviors of both the IBFM and HFB PECs a signature of the phase transition in the odd-A Eu isotopes at the mean-field level. Similar observations seem to hold for the results for the odd-A Sm isotopes, which are shown on the right-hand side of Fig. 7.

Figure 8 shows the IBFM PECs for both the odd-A La and Ba isotopes, plotted for each K quantum number, $K = 1/2, 3/2, \ldots, 11/2$, and the corresponding Skyrme-HFB PECs. The IBFM PECs reproduce the trend of the HFB PECs, namely, as N increases the potentials become shallower, and location of the equilibrium minimum shifts closer to the origin $\beta = 0$. Given that these nuclei are expected to be γ soft in nature, for a more accurate analysis it is necessary to study the behaviors of the energy surfaces in both the axial β and triaxial γ deformations.

E. Energy spectra

Low-energy spectra for the even-even core nuclei, $^{148-158}$Sm and $^{128-134}$Ba, are shown in Fig. 9. The IBM calculation overall reproduces the observed energy spectra well. The ratio $R_{4/2}$ of the 4^+_1 to 2^+_1 excitation energies serves as an indicator of the shape transition. The measured $R_{4/2}$ ratios are 2.15, 2.32, 3.00, 3.30, 3.29, and 3.29 for $^{148-158}$Sm, respectively. The $R_{4/2}$ value for ^{148}Sm is close to the vibrational U(5) limit ($R_{4/2} = 2$), and those for ^{154,156,158}Sm are close to the value in the rotational SU(3) ($R_{4/2} = 10/3$) limit. The present calculation reproduces this systematic, with the calculated $R_{4/2}$ values being 2.49, 2.79, 3.13, 3.29, 3.32, and 3.34 for $^{148-158}$Sm, respectively. The overestimates of $R_{4/2}$ in the nearly spherical, U(5), regime are due to the fact that the HFB PECs exhibit a rather large deformation, $\beta_e = 0.10$ and 0.15 for ^{148,150}Sm, respectively, and the potential is very steep. These features of the PECs are supposed to be reflected in the final IBM spectra, which have the $R_{4/2}$ ratios significantly larger than 2.0.

One can see from Figs. 9(c) and 9(d) that the mapped IBM calculations reproduce the overall systematic of the yrast levels in the even-even Ba nuclei with $72 \leqslant N \leqslant 76$, but the predicted 0^+_2 and 2^+_2 energies exhibit decreasing patterns with N in contrast to the observed ones, which gradually increase in energy. For ^{128}Ba and ^{130}Ba, the 0^+_2 and 2^+_2 excitation energies are also overestimated in the present calculation, and the level structure of these nuclei rather resembles that of rotational spectra. The mapped IBM qualitatively reproduces the increases of the 2^+_1, 4^+_1, 0^+_2 and 2^+_2 energy levels from $N = 76$ to 78. The order of levels is reasonably reproduced for ^{132}Ba and ^{134}Ba, in which the 2^+_2 levels are lying close to the 2^+_1 ones, a signature of γ softness.

Figure 10(a) shows the predicted low-energy spectra of negative-parity yrast states in odd-A $^{149-159}$Eu, obtained from the IBFM, with the Hamiltonian parameters specified by the EDF inputs using the procedure described in Sec. II. One of the empirical signatures of the possible QPTs in odd-A nuclei is a change in the spin of the lowest-energy state of a given parity at a particular nucleon number [48]. In the present case, the observed energy spectra, shown in Fig. 10(b), exhibit such a feature, as the spin I of the lowest-lying negative-parity state changes from $11/2^-$ to $5/2^-$ at $N = 90$. The mapped IBFM consistently reproduces this trend. In addition, the $11/2^-$ yrast states in ^{149}Eu and ^{151}Eu are mostly accounted for by the proton $1h_{11/2}$ single-particle configuration coupled to the weakly-deformed even-even core, and the bands based on the $11/2^-_1$ state show the $\Delta I = 2$ sequence of levels, connected by dominant $E2$ transitions. The level structure clearly changes at $N = 90$, since the yrast levels in those Eu nuclei with $N \geqslant 90$ rather resemble a rotational band following a $\Delta I = 1$ sequence. The present mapped IBFM reasonably reproduces these level structures, but overestimates the lower-spin states, e.g., with $I = 1/2^-$ and $3/2^-$. These low-spin states could probably arise from the correlations that are not incorporated in the present implementation of the IBFM, such as configuration mixing.

We also show in Fig. 10 the predicted energy levels of the positive-parity yrast states in $^{149-159}$Sm. These

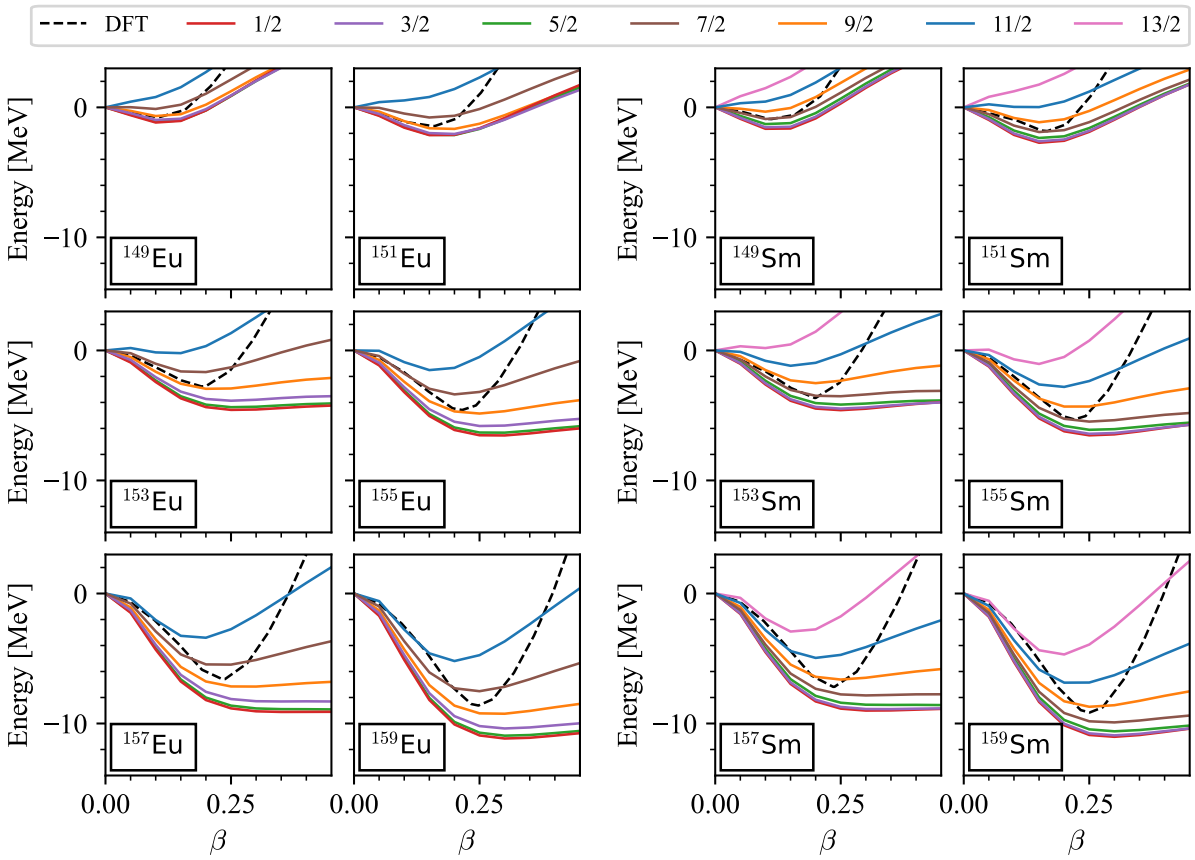

FIG. 7. Potential energy curves for the odd-A nuclei, $^{149-159}$Eu and $^{149-159}$Sm, calculated in the IBFM (solid curves) for the quantum number $K = 1/2, 3/2, \ldots, 11/2$ (for Eu) and $K = 1/2, 3/2, \ldots, 13/2$ (for Sm). The dashed curves represent the Skyrme-HFB PECs.

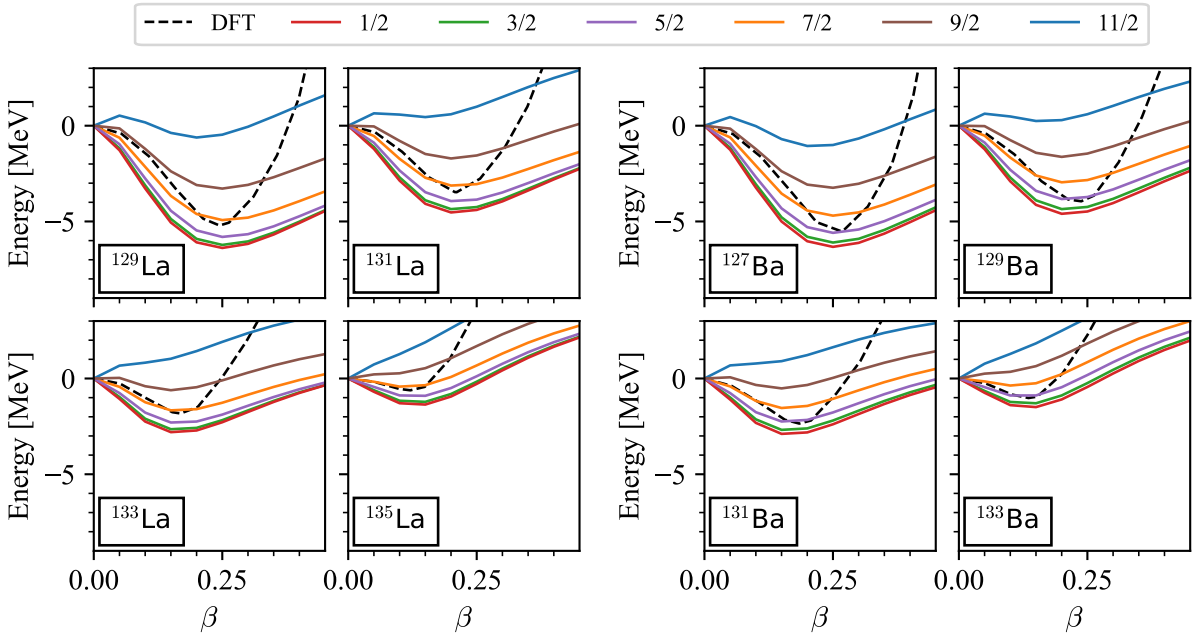

FIG. 8. Same as Fig. 7, but for $^{129-135}$La and $^{127-133}$Ba.

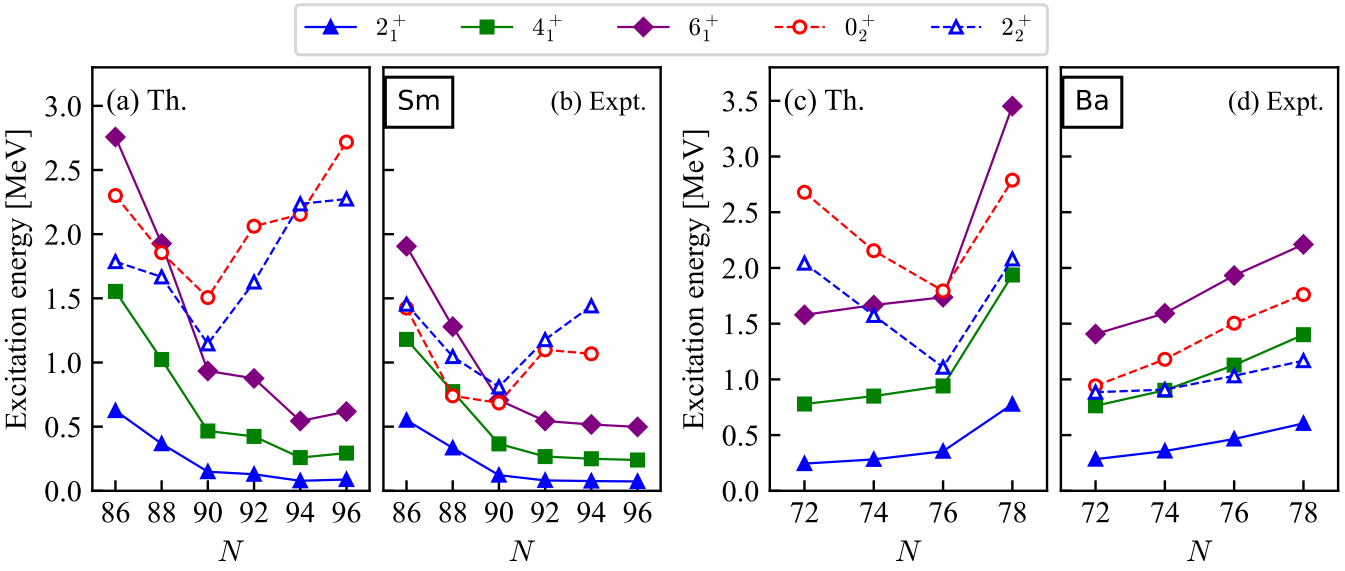

FIG. 9. Calculated and experimental [64] low-energy spectra for the even-even nuclei $^{148-158}$Sm and $^{128-134}$Ba.

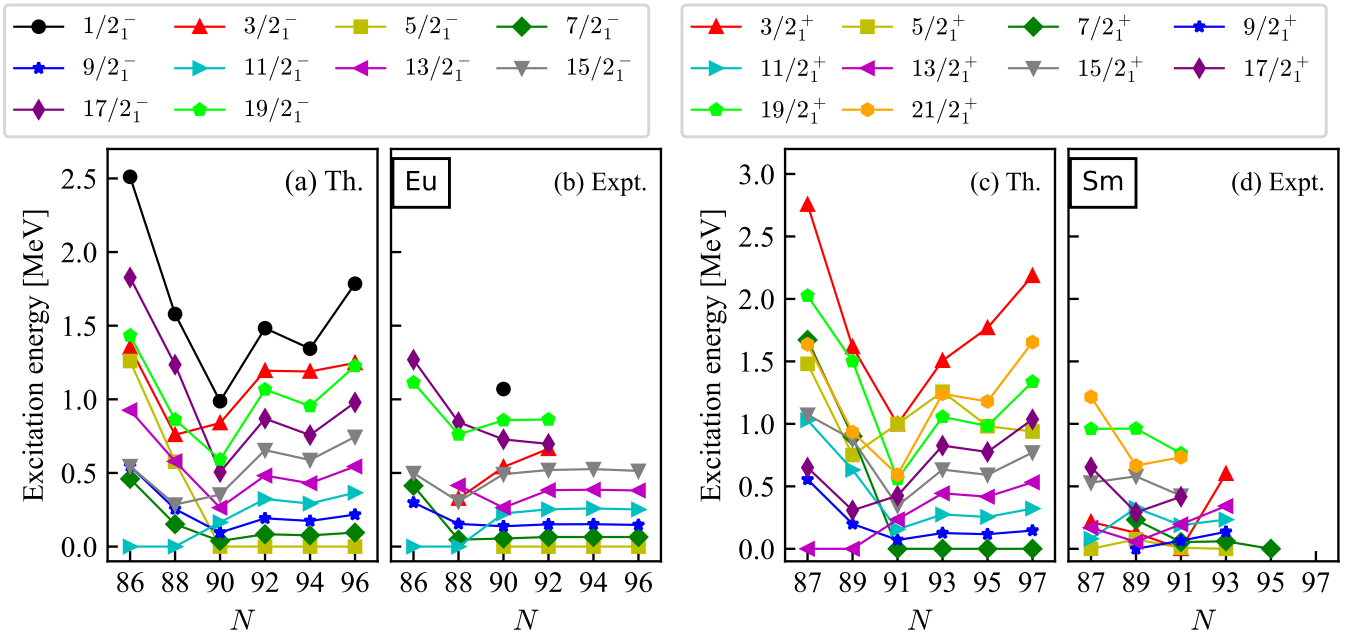

FIG. 10. Calculated and experimental [64] low-energy spectra of odd-A Eu and Sm.

states arise from the coupling of the neutron $1i_{13/2}$ single-particle state to the even-even Sm cores in the IBFM. Similarly to the odd-A Eu case, the mapped IBFM predicts the spin I of the lowest-lying positive-parity states in ^{149}Sm and ^{151}Sm to be $13/2^+$, and the subsequent $\Delta I = 2$ bands. For those odd-A Sm nuclei with $N \geqslant 91$, the calculation suggests the $\Delta I = 1$ rotational-like bands built on the $7/2^+$ states. The spectroscopic data for the odd-A Sm, however, show a much more complicated level structure than those for the odd-A Eu. In particular, the lowest-lying level structure in transitional nuclei such as those with $N = 89$ and 91 is characterized by coexistence of several decoupled, $\Delta I = 2$, and strongly-coupled, $\Delta I = 1$, bands lying quite close in energy. The present IBFM calculation is not able to reproduce full details of the observed energy spectra in the odd-A Sm, including the behavior of the $5/2_1^+$ level, which appears in the vicinity of the lowest-lying state experimentally.

In Fig. 11 the predicted excitation energies of negative-parity yrast states in $^{129-135}$La and $^{127-133}$Ba are com-

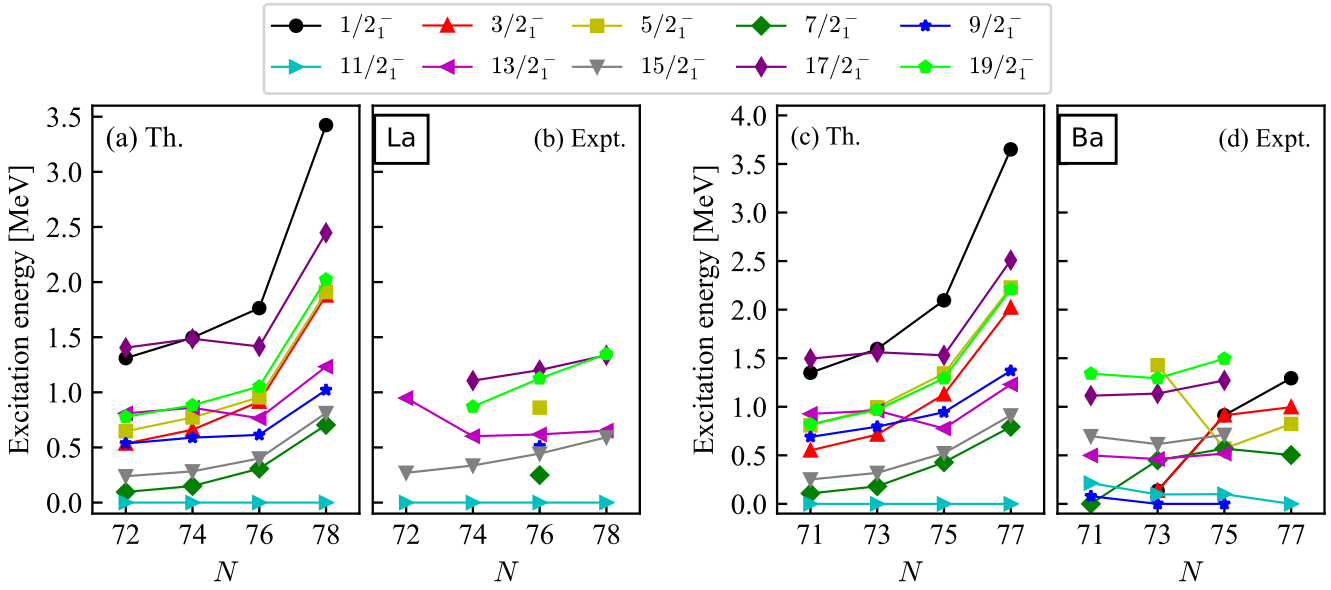

FIG. 11. Same as the caption to Fig. 10, but for odd-A La and Ba.

pared with the experimental data. Our calculation suggests the lowest-lying negative-parity state to be $11/2^-$ for all the odd-A La, and produces a gradual increase of the $I = 15/2^-$ level with N consistently with experiment. The predicted energy spectra for the odd-A La isotopes show an overall gradual increase as N approaches the neutron major shell closure $N = 82$. Note that the overestimate of the energy levels of ^{135}La could be attributed to the irregular behaviors of some of the IBM parameters at $N = 78$, in particular, the large d-boson energy, ϵ_d, obtained for ^{134}Ba [see Figs. 6(a) –6(d)].

Patterns of the low-energy negative-parity spectra for the odd-A Ba, shown on the right-hand side of Fig. 11, look similar to those in the odd-A La. Namely, in both isotopic chains the $I = 11/2^-$ state is the lowest-lying state, and the whole energy spectrum becomes more stretched as N increases. The predicted energy levels, except for that of the $9/2^-$ state, are in most cases consistent with the experimental counterparts. The evolution of the energy levels in the odd-A La and Ba appears to occur only gradually, and is not as pronounced as in the case of the rare-earth region.

F. E2 transitions

$E2$ transition properties are calculated by using the transition operator that is given as

$$\hat{T}^{(\mathrm{E2})}_{\mathrm{BF}} = \hat{T}^{(\mathrm{E2})}_{\mathrm{B}} + \hat{T}^{(\mathrm{E2})}_{\mathrm{F}} \ , \tag{23}$$

where the first and second terms represent the contributions from the even-even boson core and odd fermion, and are given, respectively, as

$$\hat{T}^{(\mathrm{E2})}_{\mathrm{B}} = e_{\mathrm{B}}\hat{Q} \tag{24}$$

$$\hat{T}^{(\mathrm{E2})}_{\mathrm{F}} = -e_{\mathrm{F}}\frac{1}{\sqrt{5}}\gamma_{jj}[a^\dagger_j \times \tilde{a}_j]^{(2)} \ . \tag{25}$$

e_{B} and e_{F} are bosonic and fermionic effective charges, respectively. The operator $\hat{Q}$ in (24) is the same quadrupole operator with the same χ parameter as those in the IBM Hamiltonian (2). The factor γ_{jj} is defined in (8). In most IBM calculations, the effective charges e_{B} are usually determined so as to reproduce the experimental $B(E2)$ values, and are also taken to be constant in a given isotopic chain. Here we assume e_{B} to be dependent on nucleon numbers, and determine its values by means of the prescription of Ref. [65] relating the $E2$ reduced matrix element to the deformation β as

$$\beta_e = \frac{4\pi}{3ZR_0^2}\sqrt{B(E2;0_1^+ \to 2_1^+)} \ , \tag{26}$$

where the β_e value is obtained from the HFB PEC, $B(E2;0_1^+ \to 2_1^+)$ is calculated in the IBM, and $R_0 = 1.2A^{1/3}$ fm. The above formula gives the value of e_{B}:

$$e_{\mathrm{B}} = \frac{3ZR_0^2\beta_e}{4\pi|\,\langle 2_1^+||\hat{Q}||0_1^+\rangle\,|} \ . \tag{27}$$

The resultant e_{B}'s for each even-even and odd-A nucleus are given in Tables II and III. The proton and neutron effective charges, $e_{\mathrm{F}} = 1.5\,e$b and $e_{\mathrm{F}} = 0.5\,e$b, respectively, which are widely used in the nuclear shell model calculations, are adopted for the fermionic operator $\hat{T}^{(E2)}_{\mathrm{F}}$ (25).

The calculated $B(E2;2_1^+ \to 0_1^+)$ values for the even-even nuclei $^{148-154}$Sm, with e_{B} being determined by using the formula (27), are 17 Weisskopf units (W.u.), 34

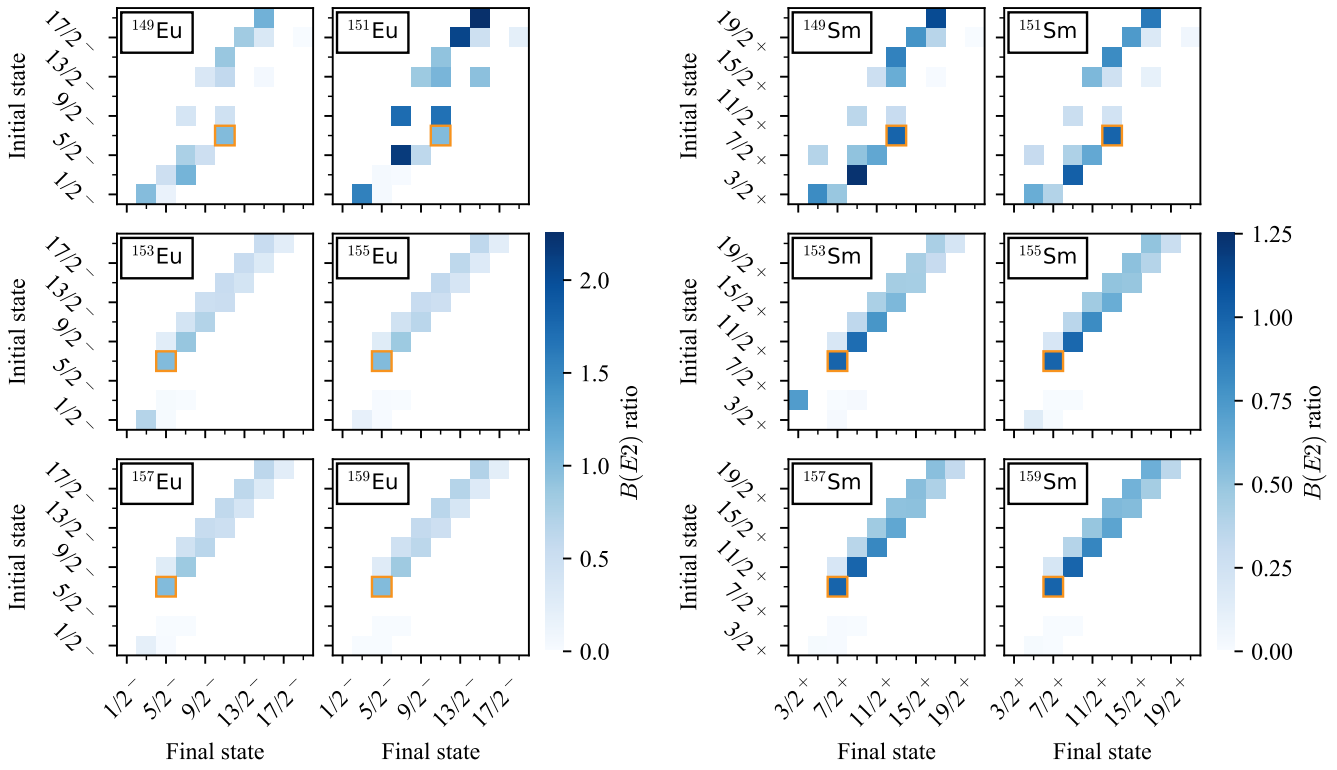

FIG. 12. Predicted $B(E2)$ values in $^{149-159}$Eu and $^{149-159}$Sm, normalized with respect to those $E2$ transitions from the second-lowest-energy state to the lowest-energy state of a given parity (marked by the thick square in each plot).

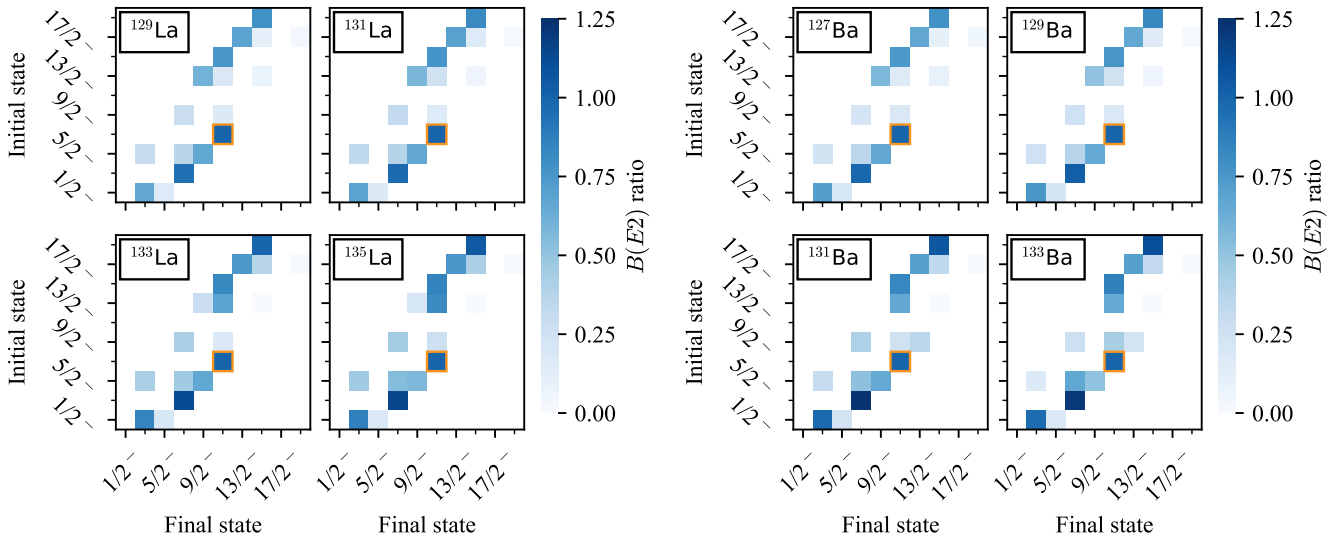

FIG. 13. Same as the caption to Fig. 12, but for $^{129-135}$La and $^{127-133}$Ba.

W.u., 51 W.u., and 99 W.u., respectively. These values are lower than those of the experimental data [64] by a factor of 2 to 3: 30.7 ± 1.5 W.u., 57.0 ± 1.3 W.u., 143.683 ± 0.087 W.u., and 177.3 ± 1.8 W.u., respectively. This is due mainly to the too small effective charges $e_{\rm B}$ derived for the even-even Sm nuclei (cf. Table II). The calculated $B(E2; 2_1^+ \to 0_1^+)$ values for $^{128-134}$Ba are 72 W.u., 51 W.u., 30 W.u., and 13 W.u., respectively, which compare rather well the experimental values [64], 72 ± 7 W.u., 57.9 ± 1.7 W.u., 43 ± 4 W.u., and 33.6 ± 0.6 W.u., respectively.

Figure 12 depicts in a color map the predicted $B(E2)$

TABLE II. Bosonic effective charges in eb units for the even-even $^{148-158}$Sm isotopes adopted in the present calculation, which are used for the odd-A Eu and Sm.

N	86	88	90	92	94	96
$e_{\rm B}$	0.068	0.085	0.092	0.092	0.124	0.145

TABLE III. Same as the caption to Table. II, but for the even-even $^{128-134}$Ba, and the neighboring odd-A La and Ba isotopes.

N	72	74	76	78
$e_{\rm B}$	0.115	0.113	0.102	0.080

values for the transitions between the negative-parity yrast states and between the positive-parity yrast states in the considered odd-A Eu and Sm nuclei, respectively. These $B(E2)$ values are normalized with respect to those of the $E2$ transitions from the second-lowest- to lowest-energy states of a given parity: $B(E2;7/2^-_1 \rightarrow 11/2^-_1)$ = 23 W.u. and 22 W.u. for ^{149,151}Eu, $B(E2;7/2^-_1 \rightarrow 5/2^-_1)$ = 68 W.u., 101 W.u., 307 W.u., and 417 W.u. for $^{153-159}$Eu, $B(E2;9/2^+_1 \rightarrow 13/2^+_1)$ = 21 W.u., and 59 W.u. for ^{149,151}Sm, and $B(E2;9/2^+_1 \rightarrow 7/2^+_1)$ = 56 W.u., 86 W.u., 272 W.u., and 376 W.u. for $^{153-159}$Sm, respectively.

In Fig. 12, for ^{149}Eu and ^{151}Eu the $B(E2)$'s for the $\Delta I = 2$ transitions, $19/2^-_1 \rightarrow 15/2^-_1$ and $15/2^-_1 \rightarrow 11/2^-_1$, are large compared with those of the $\Delta I = 1$ $E2$ transitions. There appear to be certain degrees of mixing particularly among those states with mid-spin, i.e., $I \approx 9/2$, which exhibit dominant $\Delta I = 1$ transitions. For $^{153-159}$Eu, the dominant $B(E2)$ values between states whose spins differ by 1 show the typical rotational band following the $\Delta I = 1$ systematic. Similar $B(E2)$ systematic is obtained for the odd-A Sm isotopes, which is presented on the right-hand side of Fig. 12.

We compare in Table IV predicted $B(E2)$ and spectroscopic quadrupole moments $Q(I)$ for the odd-A Eu and Sm with the experimental data [64]. There are only a few experimental data to compare for the negative-parity states in odd-A Eu. For ^{151}Eu, only the lower limit of $B(E2;9/2^-_1 \rightarrow 7/2^-_1) \geqslant 70$ W.u. is known experimentally. Our calculation gives $B(E2;9/2^-_1 \rightarrow 7/2^-_1) = 37.9$ W.u. for this nucleus, underestimating the experimental lower limit by a factor of 2. This discrepancy is considered to be due to the too small bosonic effective charge $e_{\rm B}$ for the boson core nucleus ^{150}Sm, which is here derived by the relation in (27) using the β_e value provided by the Skyrme-HFB calculation. The same seems to be true for the $B(E2;17/2^-_1 \rightarrow 13/2^-_1)$ for ^{153}Eu and $B(E2;5/2^+_1 \rightarrow 9/2^+_1)$ for ^{151}Sm. The IBFM gives a smaller quadrupole moment $Q(3/2^+_1)$ than the observed one, but the correct sign is obtained.

Figure 13 gives a plot similar to Fig. 12, but in the case of the odd-A La and Ba nuclei. The $B(E2)$ values shown in Fig. 13 are those normalized with respect to $B(E2;7/2^-_1 \rightarrow 11/2^-_1)$ = 140 W.u., 93 W.u., 39 W.u., and 17 W.u. for $^{129-135}$La, and $B(E2;7/2^-_1 \rightarrow 11/2^-_1)$ = 138 W.u., 87 W.u., 34 W.u., and 15 W.u. for $^{127-133}$Ba, respectively. We can see that in general all the odd-A La and Ba isotopes studied here indicate dominant $\Delta I = 2$ $E2$ transitions. As in the case of the weakly deformed odd-A Eu and Sm with mass $A \leqslant 151$, shown in Fig. 12, there appear to be certain mixing among low- and mid-spin states. The predicted $B(E2)$ values for some transitions in the odd-A La by the mapped IBFM are compared with the measured values in Table IV. The IBFM reproduces the observed $B(E2)$ values fairly well. The $B(E2)$ values obtained from the IBFM for ^{129}Ba are more or less consistent with the data. The present model calculation, however, gives the negative spectroscopic quadrupole moments for ^{127}Ba, ^{131}Ba, and ^{133}Ba at variance with the experimental data. This arises because the underlying Skyrme-HFB PECs for the even-even Ba cores show a rather pronounced prolate deformation (see Fig. 8), and the resulting parameter χ is negative in sign.

The deficiencies in descriptions of the electromagnetic transition properties in the odd-A nuclei, including the $B(E2)$ values for Sm and Eu being underestimated, and the incorrect sign for the spectroscopic quadrupole moments in La and Ba, could be naturally attributed to the microscopic inputs provided by the mean-field calculations, since in the present theoretical framework they influence significantly the boson effective charges (27) and the values of the IBFM parameters, in particular, the parameter χ in the boson-core Hamiltonian, which determines, to a large extent, the sign of the quadrupole moments. In addition, some interaction terms in the IBM Hamiltonian that potentially have impacts on the electromagnetic transitions may have been missing in the present calculation. For instance, as pointed out, the inclusion of the triaxial degree of freedom and cubic interactions in the mapping procedure could influence the predicted values of the $E2$ transition properties in γ-soft nuclei.

IV. SUMMARY AND CONCLUSIONS

We have developed a novel EDF-based collective model for the quantitative and systematic calculations of the spectroscopic properties in odd-A nuclei. The parameters for the IBFM, which provides spectroscopy of odd-A nuclei, have been completely determined by using the solutions of the SCMF calculations based on the nuclear EDF: the boson-core Hamiltonian is specified by mapping the EDF-SCMF potential energy onto the expectation value of the IBM Hamiltonian; the boson-fermion coupling constants are derived by associating the deformed single-particle spectra in the intrinsic frame of the IBFM with the SCMF counterparts. By extending the preceding work of Ref. [45], we here studied system-

TABLE IV. Predicted $B(E2)$ values (in W.u.) and $Q(I)$ (in eb) moments of the odd-A Eu, Sm, La, and Ba isotopes in comparison with the experimental data taken from Refs. [64, 66].

Nucleus	Properties	IBFM	Expt.
^{151}Eu	$B(E2; 9/2_1^- \to 7/2_1^-)$	37.9	> 70
^{153}Eu	$B(E2; 17/2_1^- \to 13/2_1^-)$	36.6	196^{+36}_{-31}
^{151}Sm	$B(E2; 5/2_1^+ \to 9/2_1^+)$	60.1	170 ± 30
^{153}Sm	$Q(3/2_1^+)$	$+0.497$	$+1.30 \pm 0.12$
^{129}La	$B(E2; 15/2_1^- \to 11/2_1^-)$	105	107 ± 5
	$B(E2; 19/2_1^- \to 15/2_1^-)$	109	100 ± 15
^{131}La	$B(E2; 15/2_1^- \to 11/2_1^-)$	70.5	87 ± 3
	$B(E2; 19/2_1^- \to 15/2_1^-)$	75.0	87 ± 10
^{127}Ba	$Q(7/2_1^-)$	-1.03	$+1.62 \pm 0.13$
^{129}Ba	$B(E2; 15/2_1^- \to 11/2_1^-)$	66.4	54.5 ± 2.3
	$B(E2; 19/2_1^- \to 15/2_1^-)$	71.9	90 ± 40
^{131}Ba	$Q(9/2_1^-)$	-0.534	$+1.46 \pm 0.13$
^{133}Ba	$Q(11/2_1^-)$	-0.632	$+0.89 \pm 0.07$

atically the low-lying structure in the odd-Z $^{149-159}$Eu and odd-N $^{151-159}$Sm nuclei, in which the shape phase transitions from nearly spherical to strongly deformed are expected to occur, and in the odd-Z $^{129-135}$La and odd-N $^{127-133}$Ba nuclei in the region in which γ-soft shapes are likely to emerge.

It was demonstrated that the energy spectra of the odd-A nuclei as well as those of the even-even core nuclei were calculated only by references to the microscopic inputs provided by the nuclear EDF, hence no phenomenological fit of the model parameters to experiment is required. Our microscopic IBFM reproduced quantitatively the observed energy spectra in the odd-Z Eu and, in particular, reproduced the change of spin of the lowest-lying negative-parity state near $N = 90$ as a signature of the possible QPT. Our calculation suggested a gradual evolution of the energy spectra with N in the odd-A La and Ba that is consistent with the experimental data, and indicates a shape phase transition from γ soft to nearly spherical regimes. We further devised a way of calculating the $E2$ transition probabilities with the boson effective charges determined without directly comparing to the experimental $B(E2)$ data. This provides insights into the band structure and electromagnetic transition properties in odd-A systems, for which the $B(E2)$ data are scarce.

These results demonstrate the validity of the proposed method in the general quadrupole collective states, namely, spherical vibrational U(5), deformed rotational SU(3), and γ-unstable O(6) limits, in the presence of the odd fermion in a single-j orbit. It was, however, also found that the detailed energy-level structure in odd-N Sm and Ba isotopes was not accurately described. Hwever, we consider these results for the odd-N systems to be rather reasonable, given that the IBFM calculations are here not specifically adjusted to data, but are based only on the EDF inputs. In addition, a more complete description of the γ-soft nuclei should explicitly take into account the triaxial degree of freedom and subsequently the cubic interactions in the boson core Hamiltonian. The EDF-IBFM framework in its present stage is able to capture gross systematic trends of the low-energy spectra in the odd-A γ-soft nuclei that are consistent with experiment.

Since the formalism presented in this article was limited to single-j cases, a straightforward extension would be to include multiple orbits of normal parity in the single-particle space. For the positive-parity states in odd-A Eu, for instance, there are plenty of spectroscopic data including those for the $E2$ properties, which will be useful to test the proposed methodology. Another directions of the future study concern inclusion of the neutron and proton boson degrees of freedom, i.e., an extension to the IBFM-2, for a more realistic calculation. This extension would be especially crucial for predicting nuclear processes such as β decay. In addition to the quadrupole mode, the octupole degree of freedom is expected to be relevant to determine nuclear structure in radioactive odd-A nuclei in certain mass regions of the nuclear chart. It is, therefore, an interesting subject to incorporate the octupole correlations in our model and study their influences on low-lying states in odd-A nuclei. The work along these directions will be reported elsewhere.

ACKNOWLEDGMENTS

The author MH acknowledges support from JST SPRING, Grant No. JPMJSP2119. The work of the author KN has been supported by JSPS KAKENHI Grant No. JP25K07293.

[1] A. Bohr and B. R. Mottelson, *Nuclear Structure* (Benjamin, New York, 1975).
[2] F. Iachello and O. Scholten, Phys. Rev. Lett. **43**, 679 (1979).
[3] F. Iachello and P. Van Isacker, *The interacting boson-fermion model* (Cambridge University Press, Cambridge, 1991).
[4] A. Arima and F. Iachello, Phys. Rev. Lett. **35**, 1069 (1975).
[5] F. Iachello and A. Arima, *The interacting boson model* (Cambridge University Press, Cambridge, 1987).
[6] F. Iachello, ed., *Interacting Bose-Fermi Systems in Nuclei* (Springer, New York, 1981).
[7] J. Jolie, S. Heinze, P. Van Isacker, and R. F. Casten, Phys. Rev. C **70**, 011305 (2004).

[8] P. Cejnar, J. Jolie, and R. F. Casten, Rev. Mod. Phys. **82**, 2155 (2010).
[9] F. Iachello, A. Leviatan, and D. Petrellis, Phys. Lett. B **705**, 379 (2011).
[10] K. Nomura, T. Nikšić, and D. Vretenar, Phys. Rev. C **94**, 064310 (2016).
[11] M. Böyükata, C. E. Alonso, J. M. Arias, L. Fortunato, and A. Vitturi, Symmetry **13**, 215 (2021).
[12] L. Fortunato, Prog. Part. Nucl. Phys. **121**, 103891 (2021).
[13] N. Gavrielov, A. Leviatan, and F. Iachello, Phys. Rev. C **105**, 014305 (2022).
[14] A. Leviatan and N. Gavrielov, Phys. Lett. B **868**, 139647 (2025).
[15] E. Maya-Barbecho and J.-E. García-Ramos, Phys. Lett. B **868**, 139724 (2025).
[16] F. Iachello, Phys. Rev. Lett. **44**, 772 (1980).
[17] A. B. Balantekin, I. Bars, and F. Iachello, Phys. Rev. Lett. **47**, 19 (1981).
[18] A. Frank, J. Jolie, and P. Van Isacker, *Symmetries in atomic nuclei* (Springer, 2009).
[19] P. Navrátil and J. Dobe, Phys. Rev. C **37**, 2126 (1988).
[20] F. Dellagiacoma and F. Iachello, Phys. Lett. B **218**, 399 (1989).
[21] N. Yoshida, L. Zuffi, and S. Brant, Phys. Rev. C **66**, 014306 (2002).
[22] J. Ferretti, J. Kotila, R. I. M. n. Vsevolodovna, and E. Santopinto, Phys. Rev. C **102**, 054329 (2020).
[23] K. Nomura, Phys. Rev. C **109**, 034319 (2024).
[24] M. Homma and K. Nomura, Phys. Rev. C **111**, 044302 (2025).
[25] N. Yoshida and F. Iachello, Prog. Theor. Exp. Phys. **2013**, 043D01 (2013).
[26] K. Nomura, Phys. Rev. C **105**, 044301 (2022).
[27] R. I. Magaña Vsevolodovna, E. Santopinto, and R. Bijker, Phys. Rev. C **106**, 044307 (2022).
[28] T. Otsuka, A. Arima, F. Iachello, and I. Talmi, Phys. Lett. B **76**, 139 (1978).
[29] T. Otsuka, A. Arima, and F. Iachello, Nucl. Phys. A **309**, 1 (1978).
[30] T. Mizusaki and T. Otsuka, Prog. Theor. Phys. Suppl. **125**, 97 (1996).
[31] K. Nomura, N. Shimizu, and T. Otsuka, Phys. Rev. Lett. **101**, 142501 (2008).
[32] K. Nomura, N. Shimizu, and T. Otsuka, Phys. Rev. C **81**, 044307 (2010).
[33] K. Nomura, T. Otsuka, N. Shimizu, and L. Guo, Phys. Rev. C **83**, 041302 (2011).
[34] K. Nomura, N. Shimizu, D. Vretenar, T. Nikšić, and T. Otsuka, Phys. Rev. Lett. **108**, 132501 (2012).
[35] P. Ring and P. Schuck, *The nuclear many-body problem* (Springer, Berlin, 1980).
[36] M. Bender, P.-H. Heenen, and P.-G. Reinhard, Rev. Mod. Phys. **75**, 121 (2003).
[37] D. Vretenar, A. V. Afanasjev, G. A. Lalazissis, and P. Ring, Phys. Rep. **409**, 101 (2005).
[38] L. M. Robledo, T. R. Rodríguez, and R. R. Rodríguez-Guzmán, J. Phys. G: Nucl. Part. Phys. **46**, 013001 (2019).
[39] K. Nomura, Eur. Phys. J. A **61**, 139 (2025).
[40] O. Scholten, Prog. Part. Nucl. Phys. **14**, 189 (1985).
[41] O. Scholten and A. Dieperink, in *Interacting Bose-Fermi Systems in Nuclei*, edited by F. Iachello (Springer, 1981) pp. 343–353.
[42] T. Otsuka, N. Yoshida, P. Van Isacker, A. Arima, and O. Scholten, Phys. Rev. C **35**, 328 (1987).
[43] N. Yoshinaga, Y. D. Devi, and A. Arima, Phys. Rev. C **62**, 024309 (2000).
[44] K. Nomura, T. Nikšić, and D. Vretenar, Phys. Rev. C **93**, 054305 (2016).
[45] M. Homma and K. Nomura, Phys. Lett. B **869**, 139880 (2025).
[46] A. Leviatan, Phys. Lett. B **209**, 415 (1988).
[47] A. Leviatan and B. Shao, Phys. Rev. Lett. **63**, 2204 (1989).
[48] D. Petrellis, A. Leviatan, and F. Iachello, Ann. Phys. (N.Y.) **326**, 926 (2011).
[49] B. Bally, B. Avez, M. Bender, and P.-H. Heenen, Phys. Rev. Lett. **113**, 162501 (2014).
[50] M. Borrajo and J. L. Egido, Eur. Phys. J. A **52**, 277 (2016).
[51] E. F. Zhou, X. Y. Wu, and J. M. Yao, Phys. Rev. C **109**, 034305 (2024).
[52] Y. Li, E. F. Zhou, and J. M. Yao, Phys. Rev. C **112**, 014317 (2025).
[53] F. Iachello, Phys. Rev. Lett. **85**, 3580 (2000).
[54] R. F. Casten and N. V. Zamfir, Phys. Rev. Lett. **85**, 3584 (2000).
[55] J. N. Ginocchio and M. W. Kirson, Nucl. Phys. A **350**, 31 (1980).
[56] J. Bartel, P. Quentin, M. Brack, C. Guet, and H.-B. Hakansson, Nucl. Phys. A **386**, 79 (1982).
[57] T. H. R. Skyrme, Nucl. Phys. **9**, 615 (1958).
[58] P. Marević, N. Schunck, E. Ney, R. Navarro Pérez, M. Verriere, and J. O'Neal, Comput. Phys. Commun. **276**, 108367 (2022).
[59] T. Otsuka and N. Yoshida, JAERI-M (Japan At. Ener. Res. Inst.) Report No. 85 (1985).
[60] J. P. Delaroche, M. Girod, J. Libert, H. Goutte, S. Hilaire, S. Péru, N. Pillet, and G. F. Bertsch, Phys. Rev. C **81**, 014303 (2010).
[61] K. Nomura, R. Rodríguez-Guzmán, and L. M. Robledo, Phys. Rev. C **96**, 064316 (2017).
[62] Z. P. Li, T. Nikšić, D. Vretenar, and J. Meng, Phys. Rev. C **81**, 034316 (2010).
[63] K. Nomura, T. Nikšić, and D. Vretenar, Phys. Rev. C **96**, 014304 (2017).
[64] Brookhaven National Nuclear Data Center, http://www.nndc.bnl.gov.
[65] M. Rudigier, K. Nomura, M. Dannhoff, R.-B. Gerst, J. Jolie, N. Saed-Samii, S. Stegemann, J.-M. Régis, L. M. Robledo, R. Rodríguez-Guzmán, A. Blazhev, C. Fransen, N. Warr, and K. O. Zell, Phys. Rev. C **91**, 044301 (2015).
[66] N. Stone, At. Data Nucl. Data Tables **90**, 75 (2005).